RF IMPAIRMENTS ESTIMATION AND COMPENSATION IN MULTI-ANTENNA OFDM SYSTEMS

A Thesis

Presented to

The Graduate Faculty of The University of Akron

In Partial Fulfillment

of the Requirements for the Degree

Master of Science

Shashwat Jnawali

August, 2011

RF IMPAIRMENTS ESTIMATION AND COMPENSATION IN

MULTI-ANTENNA OFDM SYSTEMS

Shashwat Jnawali

Thesis

Approved:

Advisor
Dr. Hamid Reza Bahrami

Faculty Reader
Dr. Nathan Ida

Faculty Reader
Dr. Alex De Abreu Garcia

Department Chair
Dr. Alex De Abreu Garcia

Accepted:

Dean of the College
Dr. George Haritos

Dean of the Graduate School
Dr. George R. Newkome

Date

ABSTRACT

Modern wireless transceivers use multiple transmit and/or receive antennas, higher order modulation and large bandwidth to satisfy the high data rate requirements of voice, data and multimedia applications. As wireless systems become more complex, the need to make wireless transceivers more efficient, compact and cost effective becomes challenging. It is partly due to the impairments resulting from imperfections in analog radio frequency (RF) components that reduce the efficiency of wireless transceivers. Two of the most common impairments that significantly limit the performance of wireless transceivers are in phase and quadrature (IQ) imbalance and phase noise. These are caused by the mismatch in oscillator output and random frequency fluctuations at the I and Q branches of IQ transceivers, respectively. Low-complexity estimation and compensation techniques that can jointly remove the effect of these impairments are highly desirable.

The degrading effect of RF impairments is more pronounced in multi-input-multi-output orthogonal frequency division multiplexing (MIMO-OFDM) systems. As many of the modern and future wireless systems employ MIMO-OFDM, studying the effect of and addressing the techniques to mitigate RF impairments in these systems are essential to meet the stringent requirements of modern wireless applications.

In this thesis, a simple joint estimation and compensation technique to estimate multi-path channel, phase noise and IQ-Imbalance parameters in MIMO-OFDM systems under slow fading is proposed. A subcarrier multiplexed (SM) preamble structure to estimate the channel and impairment parameters with minimum overhead is introduced and used in the estimation of IQ-Imbalance parameters as well as the initial estimation of effective channel matrix including common phase error (CPE). We then use a novel tracking method based on the second order statistics of the inter-carrier interference (ICI) and noise to update the effective channel matrix throughout an OFDM frame. Simulation results for a variety of scenarios show that the proposed low-complexity estimation and compensation technique can efficiently improve the performance of MIMO-OFDM systems in terms of bit-error-rate (BER).

ACKNOWLEDGEMENTS

I am extremely thankful to all the people who directly or indirectly influenced in the successful completion of this thesis and completion of my graduate school by providing constant help, support and guidance in various forms.

First, I would like to express my profound gratitude towards my thesis supervisor, Dr. Hamid Bahrami for providing me the opportunity to work on this hot research topic and ushering me towards successful completion of this thesis. His kindness, motivation, emotional support and continuous encouragement were the key elements to get me through graduate school and to complete my thesis.

I am greatly honored to have Dr. Nathan Ida and Dr. Alex De Abreu-Garcia in my committee and I would like to thank them for providing valuable suggestions and comments on my thesis.

I am immensely grateful to my colleagues Sajjad Beygi, Mehdi Sadeghzadeh, Ahmad Danaee, Mohammad Eltayeb, Krishna Ram Budathoki, Mehdi Maleki and Mohammadmehdi Kafashan at the Wireless Communications Laboratory for providing valuable suggestions during the completion of my thesis.

I am largely indebted to my parents Mr. Kularaj Jnawali and Mrs. Kamala Jnawali for believing in me, supporting me and being there for me in tough times. I

would also like to thank all my friends in Akron especially Kripesh Bhattarai, Rimesh Joshi, Suman Shrestha, Rosish Shakya and Sarita Bhandari for their continuous help. Finally, I would like to thank my wife, Sanchita, with all my heart, for providing the love, care, support and understanding throughout the completion of graduate school.

TABLE OF CONTENTS

LIST OF TABLES

LIST OF FIGURES

CHAPTER I

INTRODUCTION

1.1 Motivation and background

Wireless communication networks have become more ubiquitous over the past few decades as technology has taken a quantum leap making wireless devices more affordable, portable, reconfigurable and cost-effective than ever before. Wireless communication, mobile as well as fixed, is moving towards higher data rate and spectral efficiency at reasonable cost. It can partially be achieved by using more bandwidth, but, the available frequency spectrum is scarce. To further improve data rate, the use of spectrally efficient and smart wireless technologies has been adapted for current and future wireless systems.

Pioneering work by Teletar [2] pointed out the great potential of using multiple antenna to improve capacity in wireless systems. Furthermore, using multi-carrier techniques such as orthogonal frequency division multiplexing (OFDM) [3], in conjunction with multi-input-multi-output (MIMO) techniques, provides the opportunity to exploit time, frequency and space diversity. Due to the reliable performance of OFDM in a frequency selective multipath environment and the capacity, diversity and/or multiplexing enhancement offered by MIMO technology, MIMO-OFDM has

become a clear choice for future generation wireless communication systems [4, 5].

As wireless systems continue replacing wired systems, the need to match data rates is partially fulfilled by employing large bandwidth and higher order modulation. At high frequencies, the imperfections in analog front-end become dominant and cause performance bottlenecks. The so called "Dirty RF" which refers to the adverse effects resulting from the non-ideal analog radio-frequency (RF) components are unavoidable and problematic for wireless communication systems [6]. The effect of those impairments is more pronounced for highly sensitive OFDM systems and even worse for MIMO-OFDM systems [7], [8]. Hence, it is crucial to mitigate those impairments in order to meet the requirement for high data rate and spectral efficiency in wireless systems.

1.2 Scope of the thesis

The advent of homodyne receivers (also called direct conversion or zero intermediate frequency (IF) receivers) paved the way for less complex wireless receivers by down-converting bandpass signals directly to baseband signals [9]. Although homodyne receivers have significant advantages in terms of cost, flexibility and reconfigurability, they are very sensitive to RF-impairments such as flicker noise, DC-offset, even-order distortion, non-linearities, IQ-Imbalance and phase noise [9]. In this thesis, we focus on two major impairments in MIMO-OFDM homodyne receivers, i.e., IQ-Imbalance and phase noise which are considered more harmful than others.

Homodyne receivers use inphase-quadrature (IQ) signal processing that is very sensitive to oscillator output mismatches between the I and Q branches. Since perfect oscillator output is unattainable due to manufacturing imperfections, there are always some phase and amplitude mismatches between oscillators at the I and Q branches. This imbalance is referred to as IQ-Imbalance. Although typical mismatches of only 1%-5% in amplitude and 1°-5° in phase are present in today's receivers, IQ-Imbalance still causes severe performance degradation in highly sensitive OFDM systems. It also results in constellation rotation and introduces inter-carrier interference (ICI) that becomes more problematic for high-rate wireless applications using higher order modulations [10]. In addition to IQ-Imbalance, imperfect oscillators also introduce phase noise that is caused by random frequency fluctuations at the output [11]. Phase noise also destroys orthogonality between the OFDM subcarriers by introducing ICI and rotating the signal constellation [12].

The joint effects of IQ-Imbalance and phase noise renders the system useless and to realize robust wireless systems, it is very important to jointly address and mitigate those impairments. Furthermore, the attenuation, delay and phase rotation caused by the multipath wireless channel to the signal is also equally important and should also be accounted for. Since current IC technologies allows us to implement more and more complex algorithms effectively in a single chip, mitigation of those impairments in the digital domain is more feasible than in the analog domain. Hence, joint mitigation of IQ-Imbalance and phase noise for MIMO-OFDM system in a random multipath wireless channel is the central theme of this thesis.

1.3 Literature review of related work

Since RF impairments have severe effects on system performance, several studies have been done to characterize, quantify and mitigate these impairments. An overview of RF impairments for homodyne receivers can be found in [6], [13], [14] and [15] where the nature and effects of DC-offset, LO leakage, IQ-Imbalance, even order distortion and flicker noise is discussed. In [15], analog methods to compensate for these impairments by suitably designing mixers and oscillator circuitry are presented.

In [16], advanced methods to compensate for IQ-Imbalance are discussed including adaptive interference cancellation and blind source separation. The effect and compensation methods for IQ-Imbalance in single-input-single-output (SISO) OFDM systems are discussed in [10], [17], [18] and [19]. It is pointed out that IQ-Imbalance causes interference from the mirror sub-carriers in OFDM systems. The estimation and compensation techniques based on maximum likelihood (ML), least squares (LS) and least mean squares (LMS) for both pre-FFT and post-FFT processing are also discussed with their performance evaluations. IQ-Imbalance effects and compensation methods for MIMO and MIMO-OFDM systems have been studied extensively in [20], [21], [22], [23], [24] and references therein.

Another major RF impairment, phase noise, has also gained a lot of attention in the literature in its characterization, analysis and modelling . In [11] and [25], extensive analysis and modelling of free-running as well as phase locked loop (PLL) based oscillators are given. Owing to the sensitivity of OFDM systems towards

phase noise, many researchers have studied the performance of OFDM receivers in the presence of phase noise. Detailed analysis of phase noise impaired SISO-OFDM systems can be found in [12], [26], [27], [28], [29], [30]. These studies suggest that phase noise causes common phase error (CPE) and inter-carrier interference (ICI) that destroys subcarrier orthogonality in OFDM systems. Phase noise compensation schemes for SISO-OFDM systems are discussed in [12], [31], [32], [33], [34], [35] where reduction and suppression methods for ICI as well as CPE are presented. The analysis of SISO-OFDM systems cannot be easily extended to MIMO-OFDM systems as pointed out in [36] and [37]. Nevertheless, different compensation schemes for MIMO-OFDM systems have been proposed in [37], [38],[39], [40], [41], [42].

The joint effect of IQ-Imbalance and phase noise with compensation schemes for SISO-OFDM systems can be found in [8], [43], [44]. Recently, in [45], joint compensation of IQ-Imbalance and phase noise for MIMO-OFDM systems was discussed. The proposed scheme is computationally complex as it is based on maximum likelihood (ML) detection and also has large pilot overhead that increases with increasing number of transmit-receive antennas. Since the MIMO-OFDM implementation already introduces significant complexity, it is highly desirable to devise low-complexity methods to jointly estimate and compensate IQ-Imbalance and phase noise for MIMO-OFDM systems.

Furthermore, in coherent wireless OFDM systems, known pilot signals are transmitted to help in the estimation of the wireless channel and impairment parameters. The accuracy in estimation relies on the design of these pilot signals. Some pilot

signal designs for MIMO-OFDM systems are discussed in [46], [47] and [48]. In the presence of RF impairments, those methods do not provide reliable estimation. Pilot designs for MIMO-OFDM systems considering only IQ-Imbalance or phase noise can be found in [49], [50], [51]. Although, it is generally true that utilizing pilot signals in OFDM systems enables better channel estimation, it can degrade the system performance in the presence of phase noise [42]. Until now, preamble design in the presence of both IQ-Imbalance and phase noise has not yet been discussed in the literature. This thesis also aims to fill this gap by designing a suitable pilot structure to estimate the channel and impairment parameters to mitigate impairments in MIMO-OFDM systems.

1.4 Thesis overview and contribution

This thesis primarily deals with the joint effects of IQ-Imbalance and phase noise in MIMO-OFDM systems. In Chapter II, a brief overview of signal and channel modelling for MIMO, OFDM, and MIMO-OFDM systems is presented. In Chapter III, various issues in RF processing at receivers are discussed. The primary focus is given to modelling of IQ-Imbalance and phase noise. Then, the MIMO-OFDM signal model in the presence of these impairments is discussed. In Chapter IV, a suitable preamble design is presented to effectively and jointly estimate the channel, IQ-Imbalance and phase noise parameters. A novel algorithm to effectively track the channel corrupted by phase noise that utilizes the pilot symbols in OFDM symbol is developed. The estimated parameters and tracking algorithm are then utilized to

estimate the transmitted data. The performance result of the proposed scheme is then verified through simulations in MATLAB® in Chapter V. At the end, in Chapter VI, concluding remarks and possible future work are discussed. The major contributions and important results of this thesis can be summarized as:

- Development of MIMO-OFDM system model impaired by the joint effects of IQ-Imbalance and phase noise
- Development of a suitable preamble structure with minimum overhead (utilizing two full pilot OFDM symbols) to effectively estimate channel, IQ-Imbalance and phase noise parameters
- Development of a novel tracking algorithm that uses pilot subcarriers in an OFDM symbol to track the effective channel
- Extensive performance and complexity analysis of the proposed scheme through simulation

1.5 General notations

Throughout the thesis, upper-case bold letters are used for matrices, lower-case bold letters for vectors and scalars are represented by italic letters. Operators $\star$, $\odot$ and $\oslash$ indicate convolution, element-wise multiplication and element-wise division respectively. $\{.\}^*$, $\{.\}^T$, $\{.\}^H$, $\{.\}^\dagger$ and $\{.\}^\#$ represent conjugate, transpose, hermitian transpose, pseudo-inverse and conjugate mirror operation, respectively. $\mathbf{I}_N$, $\mathbf{0}_N$ represent $N \times N$ identity and zero matrices. $E\{.\}$, $\arg\{.\}$, $\text{abs}\{.\}$ represent expectation,

argument and absolute value of the elements inside the parentheses, respectively. $|\,.\,|$ and $\|\,.\,\|$ represent absolute value and norm of a vector respectively. All signals are assumed to be complex-valued Gaussian distributed unless otherwise stated.

CHAPTER II

SYSTEM MODEL

2.1 MIMO system and channel model

Multiple-input multiple output (MIMO) systems utilize multiple transmit and receive antennas for performance enhancement through diversity and/or multiplexing gain. A typical MIMO system utilizing M_t transmit and M_r receive antennas is shown in Figure 2.1. The discrete-time input-output relation of a MIMO channel with L channel taps at time n is given by [52]

$$\mathbf{y}(n) = \sum_{l=0}^{L-1} \mathbf{G}_l(n)\mathbf{x}(n-l) + \mathbf{w}(n) \tag{2.1}$$

where $\mathbf{y}(n)$ is the $M_r \times 1$ received signal vector, $\mathbf{x}(n)$ is the $M_t \times 1$ transmitted signal vector and $\mathbf{w}(n)$ is the $M_r \times 1$ additive white Gaussian noise (AWGN) vector affecting each receiver branch such that for each $q \in \{1, .., M_r\}$, $w_q(n) \in \mathcal{CN}(0, \sigma_n^2)$ where σ_n^2 is the received noise power. $\mathbf{G}_l(n)$ is the $M_r \times M_t$ multi-path channel matrix corresponding to the l^{th} channel tap at time n. In a multipath environment by considering delay, phase shift and attenuation, the discrete-time multipath channel impulse response from the p^{th} transmit to the q^{th} receive antenna can be modelled as [53]

$$g_{q,p}(n, \tau) = \sum_{l=0}^{L-1} \alpha_l(n) e^{-j\theta_l(n)} \delta(\tau - \tau_l) \tag{2.2}$$

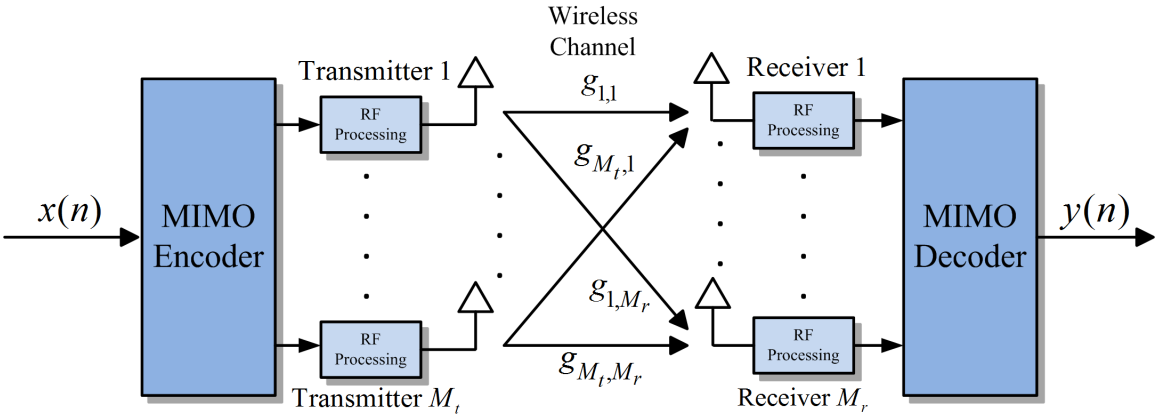

Figure 2.1: A typical MIMO system with M_t transmit and M_r receive antennas.

where α_l, θ_l and τ_l denote the attenuation, phase shift and delay corresponding to the l^{th} multipath channel tap which are time dependent. For fixed wireless systems, the time index can be dropped and can be considered constant for transmission over a certain period of time. This is sometimes called quasi-static channel assumption. The channel matrix in (2.1) can then be written as

$$\mathbf{G}(l) = \begin{bmatrix} g_{1,1}(l) & \cdots & g_{1,M_t}(l) \\ \vdots & \ddots & \vdots \\ g_{M_r,1}(l) & \cdots & g_{M_r,M_t}(l) \end{bmatrix} \tag{2.3}$$

Due to the randomly changing nature of the wireless channels, stochastic channel models are generally used to approximate the channel under study by defining various parameters such as power delay profile (PDP), root mean squared (rms) delay spread and spatial correlation [54, 55]. For instance, the response of a correlated MIMO channel can be modelled using the kronecker model with transmit and receive

correlation matrices $\mathbf{R}_t$ and $\mathbf{R}_r$ as [52]

$$\mathbf{G}(l) = \mathbf{R}_r^{1/2}(l)\mathbf{G}_w(l)\mathbf{R}_t^{H/2}(l) \tag{2.4}$$

where each element of $\mathbf{G}_w$ are independent and identically distributed complex random variables (generally following Rayleigh distribution) that depend on the propagation environment. The correlation matrices $\mathbf{R}_t$ and $\mathbf{R}_r$ can be written as

$$\mathbf{R}_t = \begin{bmatrix} 1 & \rho_t & \cdots & \rho_t^{M_t-1} \\ \vdots & \ddots & \vdots & \vdots \\ \rho_t^{M_t-1} & \cdots & \rho_t & 1 \end{bmatrix} \quad \mathbf{R}_r = \begin{bmatrix} 1 & \rho_r & \cdots & \rho_r^{M_r-1} \\ \vdots & \ddots & \vdots & \vdots \\ \rho_r^{M_r-1} & \cdots & \rho_r & 1 \end{bmatrix} \tag{2.5}$$

where ρ_t and ρ_r are the correlation coefficients with $\rho = 0$ for uncorrelated MIMO channel and $\rho = 1$ for a fully correlated MIMO channel. It is also referred to as a single coefficient spatial correlation model [55, 56]. It is also assumed that the spatial correlation matrices are the same for all the channel taps.

2.2 Orthogonal frequency division multiplexing (OFDM)

From (2.1), it can be inferred that when the channel delay spread exceeds the symbol period, the symbols overlap with each other giving rise to inter-symbol interference (ISI). This implies that the channel is not essentially frequency flat for the overall system bandwidth. To overcome this anomaly, time and/or frequency domain equalization can be used. However, especially for high data rate applications, channel equalization is computationally expensive. Multi-carrier modulation techniques like OFDM remove the need to equalize the whole broadband channel by dividing

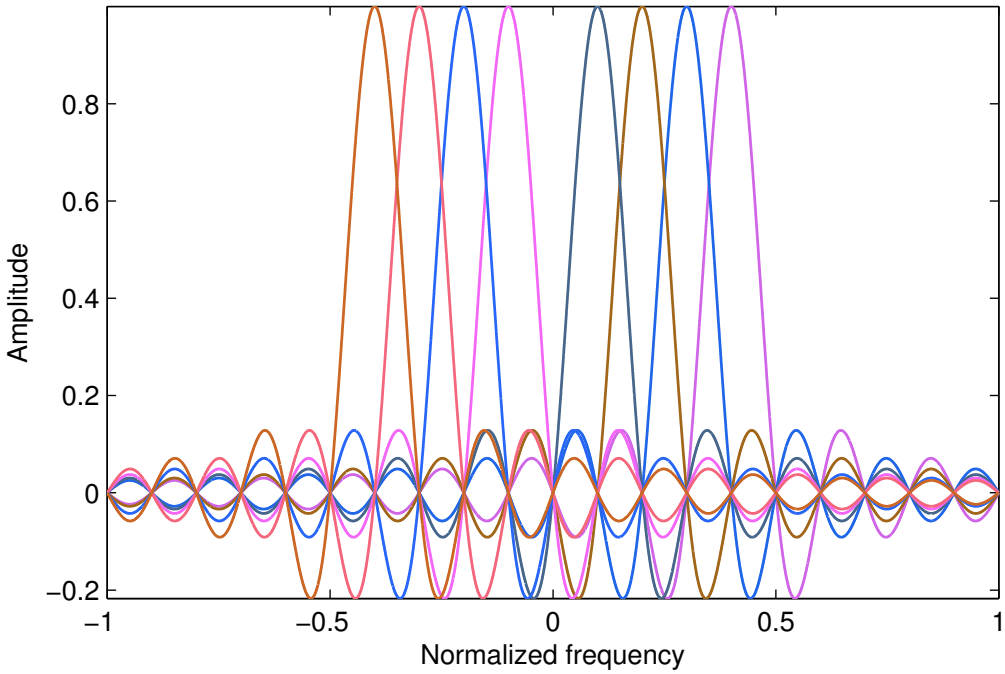

Figure 2.2: OFDM frequency spectrum with 8 orthogonal sub-carriers.

the available frequency spectrum to several narrowband orthogonal sub-channels or sub-carriers [3]. Each individual sub-carrier in an OFDM system is spaced $1/T_s$ (T_s being the symbol period) apart in frequency and can be considered frequency flat and time-invariant during the symbol transmission period thereby reducing the ISI effect significantly. A typical OFDM frequency spectrum using 8 sub-carriers is shown in Figure 2.2.

In general, to separate the sub-carriers at the receiving end, various steep bandpass filters are required. However, OFDM system can be efficiently implemented digitally using fast Fourier transform (FFT) and inverse discrete Fourier transform

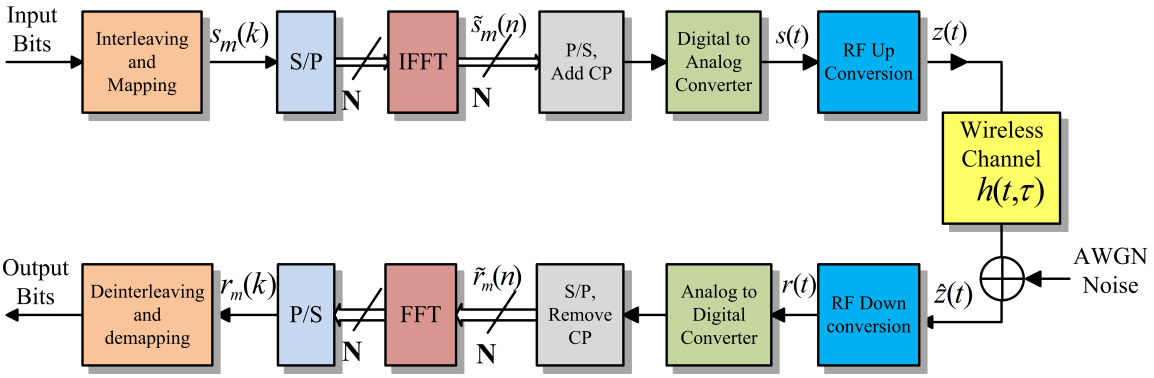

Figure 2.3: A typical OFDM system.

(IFFT). The block diagram of a typical OFDM system is shown in Figure 2.3. The frequency domain serial data signals, $\mathbf{s}_m$, corresponding to the m^{th} OFDM symbol are converted into parallel data and grouped into $N \times 1$ vectors. These data vectors are then fed into the IFFT block. The resulting time domain $N \times 1$ OFDM signal vector $\tilde{\mathbf{s}}_m$, can be written as

$$\tilde{\mathbf{s}}_m = \frac{1}{\sqrt{N}} \boldsymbol{\mathcal{F}}_N^{-1} \mathbf{s}_m \tag{2.6}$$

where $\boldsymbol{\mathcal{F}}_N^-1$ is the $N \times N$ inverse DFT matrix. The DFT matrix is given by,

$$\boldsymbol{\mathcal{F}}_N = \begin{bmatrix} 1 & 1 & 1 & 1 & 1 \\ 1 & \omega & \omega^2 & \cdots & \omega^{N-1} \\ \vdots & \vdots & \vdots & \ddots & \vdots \\ 1 & \omega^{N-1} & \omega^{2(N-1)} & \cdots & \omega^{(N-1)(N-1)} \end{bmatrix} \tag{2.7}$$

where $\omega = \exp(-j2\pi/N)$. The output of the IFFT block is then converted into serial data. In order to reduce the ISI effect resulting from multipath propagation, a guard interval (cyclic prefix (CP)) longer than the channel length ($L \leq N_{CP} \leq N$)

is appended to the beginning of the OFDM symbol. The total time domain OFDM symbol length is then $N_{tot} = N + N_{CP}$. The CP part of OFDM symbol is redundant and contains the ISI information which can be removed effectively at the receiver. After adding CP, the digital signal is converted to analog signal by using an analog to digital converter (ADC). The baseband signal is then modulated to bandpass signal and sent through the wireless channel.

The transmitted signal propagates through the channel and undergoes multipath fading. Also, AWGN gets added to the signal before it reaches the receiver. The received time domain m^{th} OFDM signal at the receiver is converted to $(N_{tot}+L-1)\times 1$ digital baseband signal $\tilde{\mathbf{r}}_m$ that can be written as

$$\tilde{\mathbf{r}}_m = \mathbf{g}_m \star \tilde{\mathbf{s}}_m + \mathbf{w}_m \tag{2.8}$$

where $\star$ denotes convolution. $\mathbf{g}_m$ is the $L\times 1$ multipath channel vector taps for the m^{th} OFDM symbol, $\tilde{\mathbf{s}}_m$ is a vector containing N_{tot} transmitted digital baseband symbols and $\mathbf{w}_m$ is the $(N_{tot}+L-1)\times 1$ AWGN vector whose entries $w_m(n) \in \mathcal{CN}(0, \sigma_n^2)$ with σ_n^2 being the received noise power. The CP part is then stripped off from $\tilde{\mathbf{r}}_m$ and the received digital signal is converted to parallel data and sent through the FFT block which brings the signal back into the frequency domain as

$$\mathbf{r}_m = \boldsymbol{\mathcal{F}}_N \tilde{\mathbf{r}}_m = \mathbf{H}_m \mathbf{s}_m + \boldsymbol{\eta}_m \tag{2.9}$$

where $\mathbf{r}_m$ is the $N \times 1$ received frequency domain signal vector, $\mathbf{s}_m$ is the $N \times 1$ transmitted frequency domain signal vector, $\tilde{\mathbf{r}}_m$ is the $N \times 1$ discrete time domain received vector. $\boldsymbol{\mathcal{F}}_N$ is the $N \times N$ DFT matrix, $\boldsymbol{\eta}_m$ is the $N \times 1$ frequency do-

main AWGN vector and $\mathbf{H}_m$ is the channel frequency response matrix which can be written as $\mathbf{H}_m = diag\{h_m(0), h_m(1), ..., h_m(N-1)\}$, where each element $h_m(k) = \sum_{l=0}^{L-1} g_m(l) \exp(-j2\pi kl/N)$ for $k = 0, 1, .., N-1$.

2.3 MIMO-OFDM system model

The application of MIMO techniques to OFDM systems provides numerous advantages including multiplexing and/or diversity gains in a frequency selective environment. MIMO techniques can be applied to the orthogonal sub-carriers in the OFDM system as presented in previous sections. A simplified block diagram depicting a MIMO system applying M_t transmit and M_r receive antennas and using OFDM with N sub-carriers is shown in Figure 2.4.

As shown in Figure 2.4, the $M_tN \times 1$ modulated input data streams corresponding to N subcarriers from M_t transmit antennas are arranged in parallel and passed through the IFFT block. The resulting $M_tN \times 1$ signal corresponding to the m^{th} OFDM symbol in time domain is

$$\tilde{\mathbf{s}}_m = (\frac{1}{\sqrt{N}} \boldsymbol{\mathcal{F}}_N^{-1} \otimes \mathbf{I}_{M_t}) \mathbf{s}_m \tag{2.10}$$

where $\otimes$ represents the Kronecker product. The time domain signal $\tilde{\mathbf{s}}_m$ is converted to serial data and CP is added to combat ISI in a multi-path environment. The digital data is then converted to analog and sent through the wireless channel after up-conversion from each M_t transmit antenna. The digital time domain m^{th} received

OFDM signal at one of the q^{th} receive antenna is as follows

$$\tilde{\mathbf{r}}_{q,m} = \sum_{p=1}^{M_t} \mathbf{g}_{q,p} \star \tilde{\mathbf{s}}_{p,m} + \mathbf{w}_q \tag{2.11}$$

where $\tilde{\mathbf{r}}_{q,m}$ is the $(N_{tot} + L - 1) \times 1$ received signal vector, $\mathbf{g}_{q,p}$ is the L tap channel impulse response of the wireless multipath channel from the p^{th} transmit to the q^{th} receive antenna, $\tilde{\mathbf{s}}_{p,m}$ is the $N_{tot} \times 1$ transmitted discrete time signal vector from the p^{th} transmit antenna and $\mathbf{w}_q$ is the vector of AWGN affecting each of the q^{th} receive antenna with each $w_q(n) \in \mathcal{CN}(0, \sigma_n^2)$.

The CP is stripped off from the received discrete time domain signal and arranged into parallel streams as a $M_r N \times 1$ signal vector, after which they are fed into the IFFT block which returns the received time domain data back into the frequency domain represented as

$$\mathbf{r}_m = (\boldsymbol{\mathcal{F}}_N \otimes \mathbf{I}_{M_r})\, \tilde{\mathbf{r}}_m = \mathbf{H}_m \mathbf{s}_m + \boldsymbol{\eta}_m \tag{2.12}$$

where $\mathbf{r}_m$ is the $M_r N \times 1$ received m^{th} frequency domain OFDM signal vector, $\mathbf{s}_m$ is the $M_t N \times 1$ transmitted m^{th} frequency domain OFDM signal vector, $\tilde{\mathbf{r}}_m$ is the $M_r N \times 1$ discrete time domain received vector, $\boldsymbol{\eta}_m$ is the $M_r N \times 1$ frequency domain noise vector and $\mathbf{H}_m$ is the channel frequency response matrix which can be written as a block diagonal matrix with each block element $\mathbf{H}_m(k) = \sum_{l=0}^{L-1} \mathbf{G}(l) \exp(-j2\pi kl/N)$ as

$$\mathbf{H}_m = \begin{bmatrix} \mathbf{H}_m(0) & \cdots & \mathbf{0} \\ \vdots & \ddots & \vdots \\ \mathbf{0} & \cdots & \mathbf{H}_m(N-1) \end{bmatrix} \tag{2.13}$$

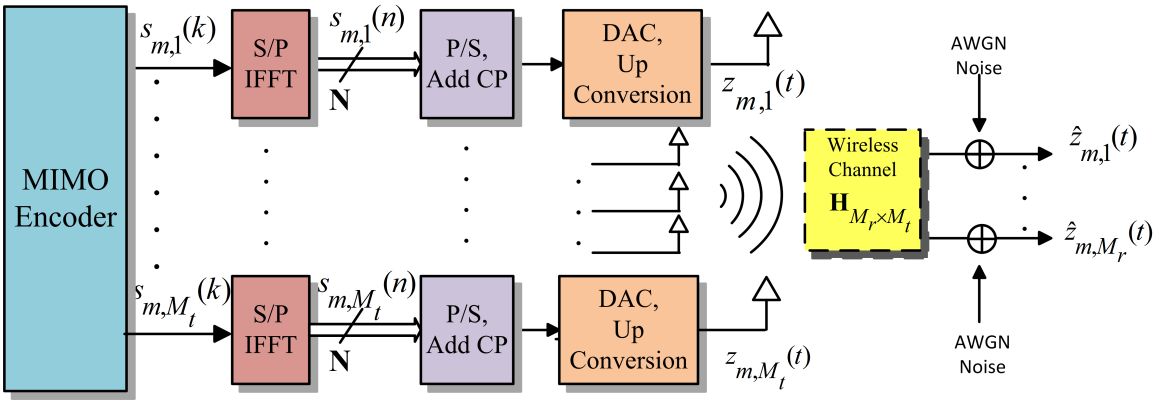

(a) MIMO OFDM Transmitter

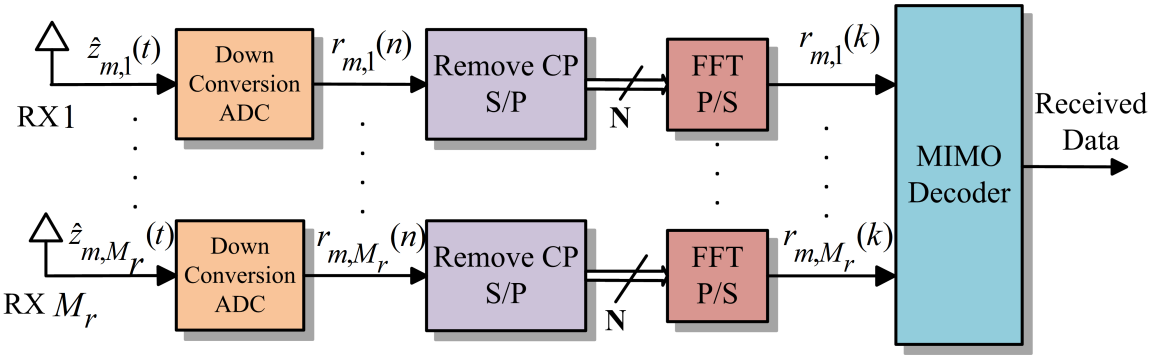

(b) MIMO OFDM Receiver

Figure 2.4: Typical MIMO-OFDM transmitter and receiver architectures

The received $M_r N \times 1$ frequency domain signal vector $\mathbf{r}_m$ in (2.12) can be written for individual k^{th} subcarrier where $k = 0, 1, .., N-1$ as

$$\mathbf{r}_m(k) = \mathbf{H}_m(k)\mathbf{s}_m(k) + \boldsymbol{\eta}_m(k) \tag{2.14}$$

where $\mathbf{r}_m(k)$, $\mathbf{s}_m(k)$, $\mathbf{H}_m(k)$ and $\mathbf{n}_m(k)$ are the $M_r \times 1$, $M_t \times 1$, $M_r \times M_t$ and $M_r \times 1$ frequency response received signal vector, transmitted signal vector, channel frequency response matrix and noise frequency response at k^{th} sub-carrier for m^{th} OFDM symbol respectively.

In this chapter, a typical MIMO-OFDM system model under multipath fading conditions and AWGN noise was discussed. To realize MIMO-OFDM transceivers in practice, various analog and digital components have to be interconnected. The complexity of these transceivers imposes several design challenges. Since ideal output from analog components such as oscillators, A/D converters and amplifiers is not practically possible, even the slightest error resulting from these components can potentially cause significant performance degradation in highly sensitive and complex transceivers such as those using MIMO-OFDM. In Chapter III, we introduce different types of impairments that result from imperfect RF components and their corresponding models and impact on a MIMO-OFDM system.

CHAPTER III

RF IMPAIRMENTS

3.1 Issues in RF processing

With increasing demand for high data rate and spectrally efficient wireless technologies, future wireless systems must cope with the cost, complexity and power requirements. Traditional RF processing techniques such as heterodyne receivers when applied to modern wireless systems impose heavy complexity burden and lack flexibility and reconfigurability. This causes performance limitations in terms of cost, gain and noise power trade-off [9]. Furthermore, it is more practical and effective to shift demanding signal processing tasks to digital baseband domain. This is mainly due to the advancements in IC technology that allows heavy computations to be done effectively and reliably with cost effectiveness, flexibility and reconfigurability. This ability to handle complex digital signal processing (DSP) in a single integrated chip has motivated recent wireless systems to switch from traditional heterodyne receivers to low intermediate frequency (IF) and homodyne (also called as direct conversion or zero-IF) receivers.

3.1.1 Receiver architecture

Modern receivers serve multiple users that operate in narrow bandwidth and require ability to select the appropriate channel with effective interference suppression from other channels. Moreover, they operate in several GHz frequency that puts a very high constraint in the filter design [9]. To this end, receivers typically convert the received signal frequency ω_r into intermediate frequency (IF), ω_{IF}, by mixing the incoming signal with a sinusoid of frequency $\omega_r - \omega_{IF}$. This mixing process generates frequency components at ω_{IF} and $2\omega_r - \omega_{IF}$. Hence, the major issue arising in this type of down conversion is the so called *image band* problem [14, 15] that is caused by the interference of the required signal with its mirror signal. To overcome this problem, image-rejection filters are applied before mixing the incoming signals with the local oscillator signal. Another method to overcome this problem is to implement complex mixing or inphase-quadrature (IQ) mixing in which the incoming signal is mixed with complex exponential ($e^{-j(\omega_r - \omega_{IF})}$) with only one frequency component (3.1). As opposed to two frequency components generated by the real mixing technique involving real sinusoid, complex mixing prevents the image band problem by generating only one desired frequency component as shown in Figure 3.2. The unwanted frequency components can then be removed using a filter to select the desired signal.

Among various receiver architectures, two widely-used and well-known receiver architectures, i.e., heterodyne and homodyne, are discussed in this section. Heterodyne receivers have been traditionally used in many applications while homo-

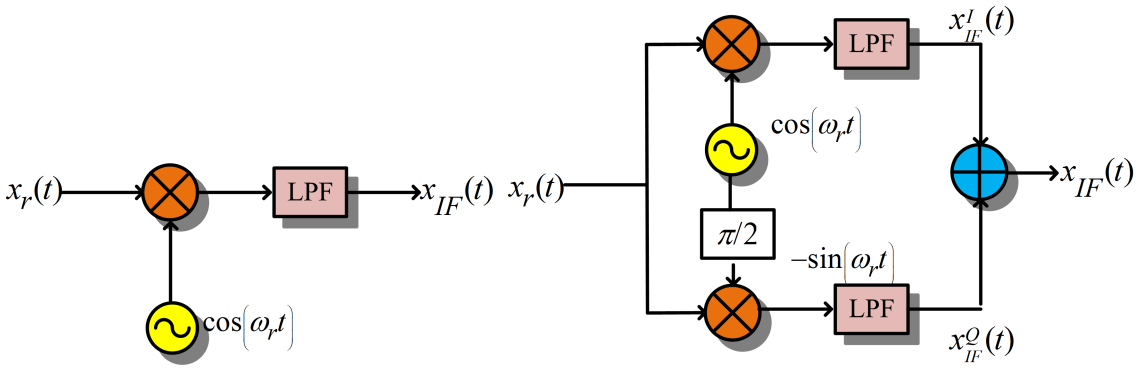

(a) Real mixing (b) Complex mixing

Figure 3.1: Real and complex mixing in analog down-converters

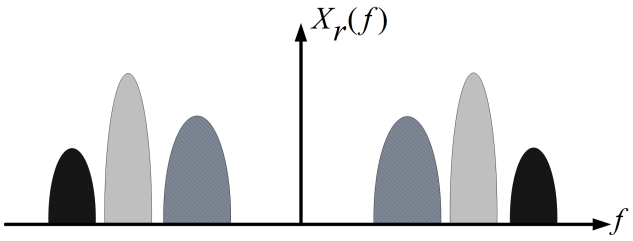

(a) RF signal spectrum

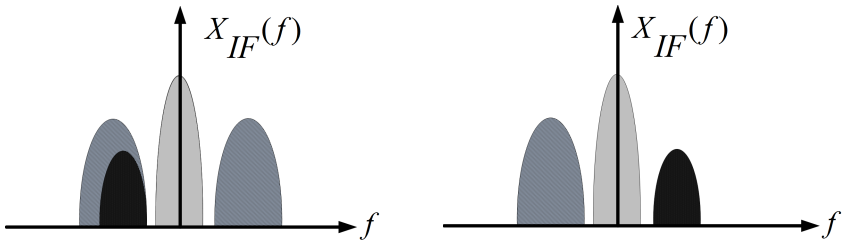

(b) Down-converted signal spectrum after real mixing

(c) Down converted signal spectrum after complex mixing

Figure 3.2: Spectrum of the received signal as a result of real and complex mixing

dyne receivers are gaining much more popularity in recent years due to the advantages they offer to future wireless systems in terms of complexity [9]. The concept of ho-

modyne receivers is not new but its application was hindered by the lack of sufficient IC technologies. In Figure 3.3, the simplified architectures of typical heterodyne and homodyne receivers are shown.

In heterodyne receivers, the incoming signal is amplified using low noise amplifier (LNA) followed by an image reject (IR) filter. The resulting signal is then mixed with local oscillator signal which performs frequency conversion. A channel selection filter is then applied to select the desired channel after which complex mixing is performed to demodulate the desired signal. The major design concern is choosing the right IF such that it is high enough to successfully reject the image band and low enough such that channel selection filters can be designed feasibly. Although this receiver architecture provides high channel selectivity, it suffers from several disadvantages such as severe trade-off between gain, noise levels, stability and power requirements [9].

On the other hand, instead of translating the frequency of the incoming signal to IF, homodyne receivers translate the incoming bandpass signal directly to baseband signal after amplifying through LNA. After IQ mixing – which is required for amplitude/phase modulated signals such as frequency modulated (FM) or quadrature amplitude modulated (QAM) signals – low pass filters can be utilized to achieve channel selectivity. This has various advantages over heterodyne receivers. It does not suffer from *image band* problem and does not require IR filters thereby hugely reducing the system complexity. The low pass filters and baseband amplifiers are perfect for integrating the receiver circuit in a single IC chip [9]. Although homodyne

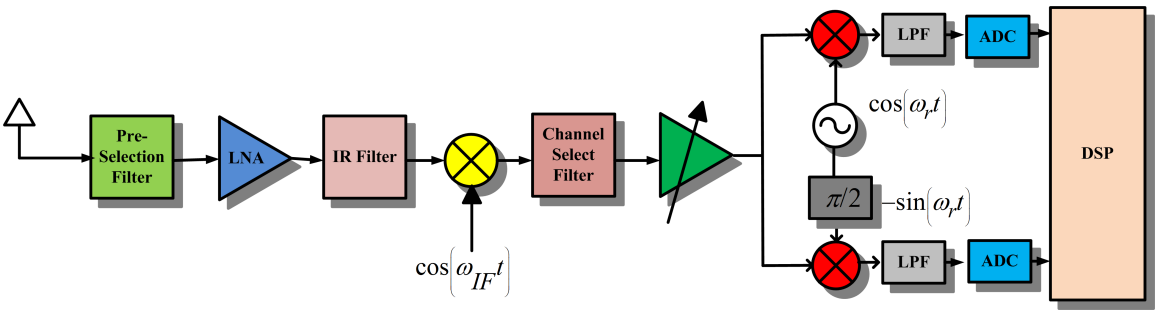

(a) Heterodyne receiver

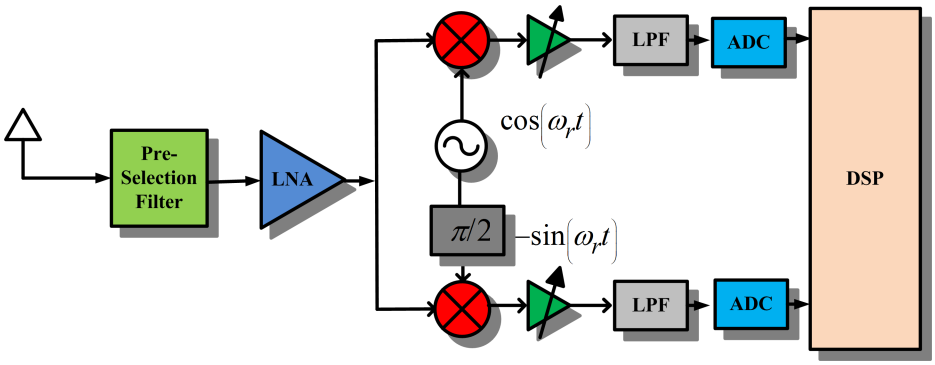

(b) Homodyne (zero-IF) or direct conversion receiver (DCR)

Figure 3.3: Heterodyne and homodyne receiver architectures

architecture is very attractive for future high rate wireless applications as compared to heterodyne architecture, it introduces various RF-impairments into the received baseband signal due to the non-ideal components.

3.2 RF impairments in receivers

The attractiveness of the homodyne architecture comes with various implementation issues that mainly arise from the impairments in analog hardware in the receiver front

ends. In this section, we discuss several impairments associated with those homodyne receivers as well as impairments for general receiver architectures.

3.2.1 DC offset, even order distortion and flicker noise

In [15, 13], various issues related to homodyne architecture are studied with possible solutions to the impairments caused by imperfections in receiver circuitry. The main issues such as DC offsets, flicker noise, even order distortion, LO leakage in the homodyne receivers are summarized below.

Direct current (DC) offset is one of the major issues in homodyne receivers. Since they down-convert the signals to DC, any additional offset voltages can cause severe problems in the received signals and saturate the following stages [9]. DC-offset arises when the mixer, local oscillator (LO) and LNA are not perfectly isolated from each other and some feedback link is present from the LO to LNA introducing DC component at the mixer output. DC offset prohibits the correct amplification of the desired signal. It must be remedied by using various techniques such as AC-coupling(High pass filtering) and offset cancellation methods which are discussed in [15] and references therein.

Homodyne receivers also suffer from even-order distortion from non-linearities arising in amplifiers and RF mixers. In the presence of high frequency interferers, they contribute to the generation of low frequency components in the presence of even order distortion [9]. A feasible solution for overcoming even order distortion is to use differential amplifiers but it fails to fully suppress it.

Furthermore, homodyne receivers also suffer from flicker noise. This type of noise is also referred to as 1/f noise or pink noise which is related to direct current [9] and is a low frequency phenomenon. Since the down-converted signal is located around DC, this noise has a significant effect on the signal to noise (SNR) ratio and causes severe problems especially in metal oxide semiconductor (MOS) RF chips. A possible solution to overcome flicker noise is to implement periodic offset cancellation through correlated double sampling [9].

3.2.2 Jitter

Jitter is the deviation or displacement of the pulses in a high frequency digital signal in high rate wireless systems [9]. It can be in terms of amplitude, phase timing, or the width of the signal pulse. Aperture jitter is the switching time variation for sample and hold circuits using analog to digital converters (ADCs) resulting in the error voltage proportional to the magnitude of the jitter. The more the input frequency and amplitude, the more the system is susceptible to the aperture jitter effects. Aperture jitter is also identified as the dominating error that limits the achievable SNR [6]. Another type of jitter is clock jitter produced by the clock generator that feeds the ADC with the clock signal. It is caused by the phase noise of the oscillator and causes the sampling time errors in ADC. The error auto-correlation function for aperture jitter depends on the sampling time difference while clock jitter depends also on absolute sampling time instants. This is why the error power for aperture jitter is a constant and is distributed over the whole band and can be suppressed by using

oversampling and filtering [6].

3.2.3 Non-linearities

The non-linear characteristics of mixer, oscillator, ADC, and power amplifier cause non-linear distortion in the received signals [6, 7]. This is more pronounced in systems using multi-carrier techniques such as OFDM. It introduces the problem of high peak to average ratio (PAPR) requiring highly linear front-end components and also increases the overall cost for the system implementation. Several solutions for overcoming impairments due to non-idealities are discussed in [7].

Detailed analysis including effects and compensation techniques of all the aforementioned impairments are out of the scope of this thesis. Hence, two major types of impairments are studied in detail in this thesis, i.e., IQ-Imbalance and phase noise.

3.3 IQ-Imbalance

Homodyne receivers using phase and frequency modulated schemes mandates the use of quadrature or IQ mixing since both the positive and negative frequency components contain signal information. As shown in Figure 3.3(b), the received RF signal after LNA block is fed into two quadrature receiver branches which requires either shifting the received RF signal or the LO signal by $\pi/2$. The more feasible way is to shift the LO signal [9]. Theoretically, these receivers provide perfect image attenuation to remove the need of image rejection filters. In practice, however, there is always

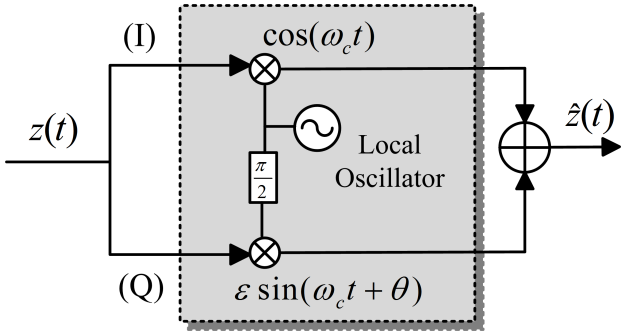

Figure 3.4: IQ receiver with phase (θ) and amplitude (ε) mismatch

some phase and amplitude mismatch in the I and Q branches of the LO commonly known as IQ-Imbalance. The typical values for IQ mismatch is between 1%-5% in amplitude and 1°-5° in phase which causes the constellation rotation of the received signals [15, 6]. IQ-Imbalance may arise in both transmitters and receivers and are also categorized as frequency-dependent and frequency-independent IQ-Imbalance [7, 16]. In this thesis, we focus on the frequency independent IQ-Imbalance at the receiver. The analysis for frequency dependent IQ-Imbalance and consideration of both transmit and receive IQ-Imbalances are left as possible future work.

3.3.1 IQ-Imbalance model

Let us consider the continuous time domain transmitted RF signal after IQ up-conversion as

$$\begin{aligned} z(t) &= 2(\Re\{s(t)\}\cos(\omega_c t) - \Im\{s(t)\}sin(\omega_c t)) \\ &= s(t)e^{j\omega_c t} + s^*(t)e^{-j\omega_c t} \end{aligned} \tag{3.1}$$

where $s(t)$ is the complex baseband signal to be transmitted and $\Re\{s(t)\} = (s(t) + s^*(t))/2$ and $\Im\{s(t)\} = (s(t) - s^*(t))/2i$ are the real and imaginary parts of the transmitted baseband signal. ω_c represents the carrier oscillator frequency. As shown in Figure 3.4, the LO output at the receiver with phase and amplitude mismatch of θ and ε, respectively, can be modelled as [6, 7, 16]

$$\begin{aligned} c(t) &= \cos(\omega_c t) - j\varepsilon \sin(\omega_c t + \theta) \quad (3.2) \\ &= K_1 e^{-j\omega_c t} + K_2 e^{j\omega_c t} \quad (3.3) \end{aligned}$$

where K_1 and K_2 are given as

$$K_1 = \frac{1 + \varepsilon e^{-j\theta}}{2} \ , \quad K_2 = \frac{1 - \varepsilon e^{j\theta}}{2} \quad (3.4)$$

The perfect amplitude and phase match between I and Q branch represents $\varepsilon = 1$ and $\theta = 0$ such that $K_1 = 1$ and $K_2 = 0$. Due to the imbalance between those branches, perfect image rejection is not available, i.e., the signals at the Q branch interfere with the I branch. To further illustrate this mathematically, let us consider that, at the receiver, the bandpass signal $z(t)$ is mixed with LO signal $c(t)$ as

$$\hat{z}(t) = z(t)c(t) = K_1 s(t) + K_2 s^*(t) + K_1 s(t) e^{2j\omega_c t} + K_2 s^*(t) e^{-2j\omega_c t} \quad (3.5)$$

After low pass filtering, we have

$$x(t) = K_1 s(t) + K_2 s^*(t) \quad (3.6)$$

Equation (3.6) in discrete time domain can be written as

$$x(n) = K_1 s(n) + K_2 s^*(n) \quad (3.7)$$

The second term in (3.7) represents the effect of IQ-Imbalance by introducing unwanted interference from the image signal. So far, we have not considered the effects of the channel and it will be discussed in the next section.

3.3.2 Effect of IQ-Imbalance in MIMO-OFDM systems

In this section, we study the IQ-Imbalance effects in MIMO-OFDM systems. First, let us consider a SISO system utilizing OFDM. The discrete time domain received m^{th} OFDM signal at the receiver including IQ-Imbalance can be written by combining equations 2.8 and 3.7 as

$$x(n) = K_1 r(n) + K_2 r^*(n) + w(n) \tag{3.8}$$

Serial to parallel conversion and FFT operation results in the frequency domain signal $\hat{x}(k)$ as

$$x(k) = K_1 r(k) + K_2 r^{\#}(k) + \eta(k) \tag{3.9}$$

where $r(k)$ is as given in equation (2.9). The operation # represents the conjugate mirror operation such that if $r(k)$ is the frequency domain signal at k^{th} subcarrier then, $r^{\#}(k) = r^*(-k)$. Extending the result from SISO case to the MIMO case by combining equations (2.14) and (3.9), we get

$$\begin{aligned} \mathbf{x}_m(k) &= \mathbf{K}_1 \mathbf{r}_m(k) + \mathbf{K}_2 \mathbf{r}_m^{\#}(k) + \boldsymbol{\eta}_m(k) \\ \mathbf{x}_m(k) &= \mathbf{K}_1 \mathbf{H}_m(k) \mathbf{s}_m(k) + \mathbf{K}_2 \mathbf{H}_m^{\#}(k) \mathbf{s}_m^{\#}(k) + \boldsymbol{\eta}_m(k) \end{aligned} \tag{3.10}$$

where $\mathbf{x}_m(k)$ is the $M_r \times 1$ received frequency domain signal suffering from IQ-Imbalance for m^{th} OFDM symbol at k^{th} subcarrier. $\mathbf{H}_m(k)$ and $\mathbf{H}_m^{\#}(k)$ are the

$M_r \times M_t$ frequency domain channel response matrices at the k^{th} and $-k^{th}$ subcarriers. $\mathbf{s}_m(k)$ and $\mathbf{s}_m^{\#}(k)$ represent the transmitted frequency domain signal for for m^{th} OFDM symbol at k^{th} and $-k^{th}$ subcarriers, respectively.

It is evident from equation (3.10) that the received signals include the desired signal and the interference from the mirror subcarriers. This happens when the IQ receiver cannot attenuate the image signal completely. The effect of IQ-Imbalance on the received 16-QAM signal constellation for a 2×2 MIMO-OFDM system at different SNR with different phase and amplitude mismatches is shown in Figure 3.5.

3.4 Phase noise

Phase noise is another type of RF impairment that is caused by random frequency fluctuations from imperfect oscillators. It results in random phase variations at the oscillator output [11]. For transceivers requiring low cost implementations and operating on high carrier frequencies, phase noise is a great performance limiting factor [12]. In this section, phase noise modelling and the effect of phase noise in multicarrier systems especially OFDM is discussed. For OFDM systems, as it will be shown, phase noise destroys the orthogonality between the subcarriers and causes the rotation of the constellation symbols. This effect makes the system unusable if not compensated effectively. We first start with the case of SISO systems and later extend it for MIMO systems.

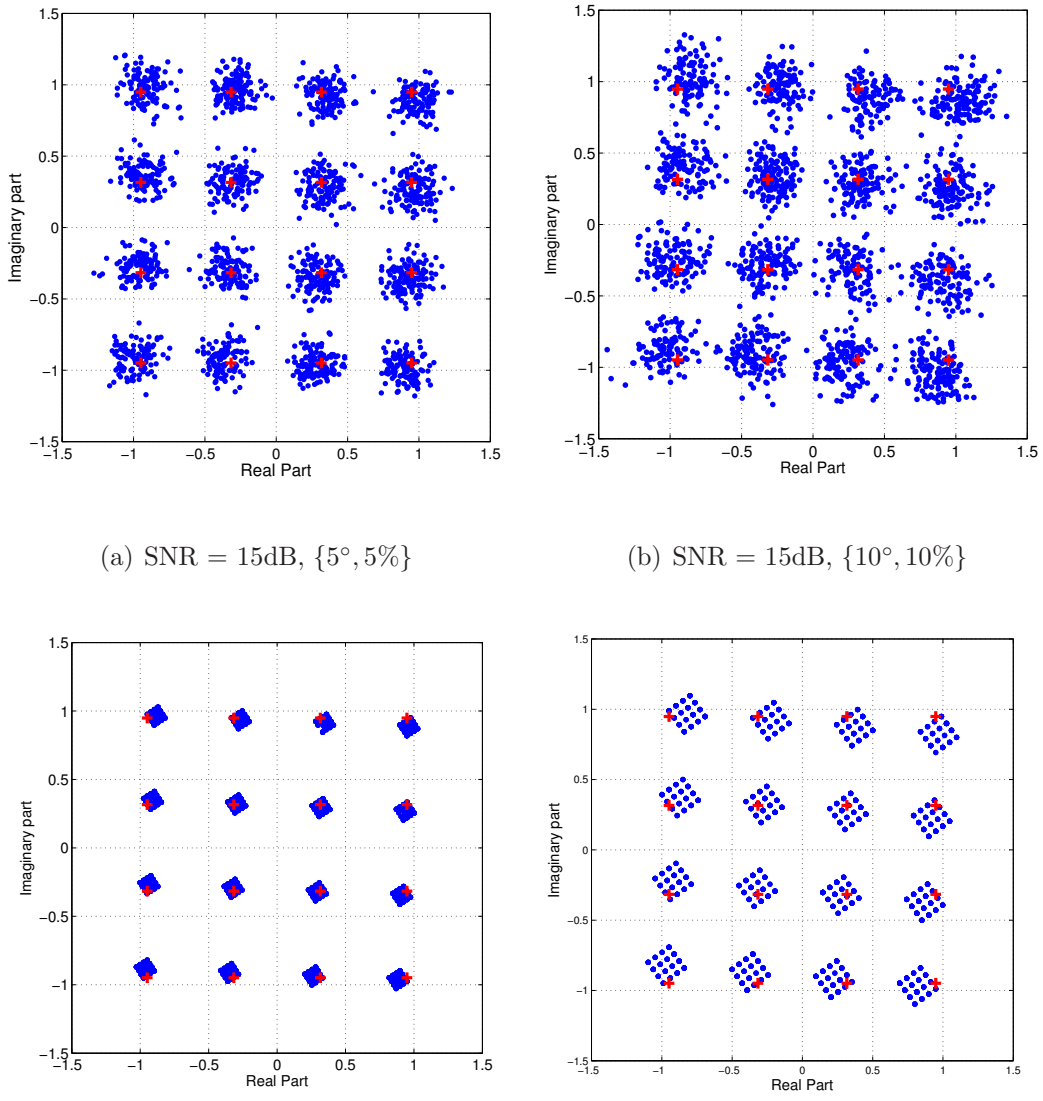

(a) SNR = 15dB, $\{5°, 5\%\}$

(b) SNR = 15dB, $\{10°, 10\%\}$

(c) SNR = 50dB, $\{5°, 5\%\}$

(d) SNR = 50dB, $\{10°, 10\%\}$

Figure 3.5: Constellation plot for 16-QAM 2×2 MIMO-OFDM system at different SNR and IQ mismatch parameters

3.4.1 Phase noise model

In presence of phase noise, the oscillator output is phase modulated with a random phase that varies with time. Considering free-running oscillator model, the continuous

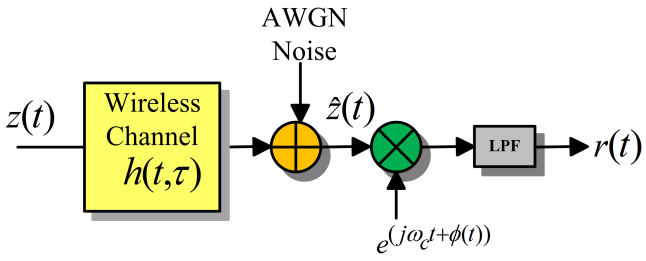

Figure 3.6: Phase noise effect on the transmitted signal

time oscillator output in presence of time variant phase noise $\phi(t)$ can be written as

$$c(t) = e^{j\omega_c t + \phi(t)} \tag{3.11}$$

In Figure 3.6, the multiplicative effect of the phase noise on a transmitted signal is depicted. The phase noise process $\phi(t)$ can be represented as a continuous time Brownian motion process with zero mean and variance that increases linearly with time [11], i.e.,

$$\sigma_\phi^2 = E\{\phi^2(t)\} = \kappa t \tag{3.12}$$

where κ is the rate of increment of variance with time. The phase noise process is then given by

$$\phi(t) = \sqrt{\kappa} B(t) \tag{3.13}$$

where $B(t)$ represents the standard Brownian motion with $B(0) = 0$. In case of perfect oscillators, the power spectral density (PSD) spectrum consists of a delta function at the required frequency but in presence of the phase noise, the oscillator output power is spread around the desired frequency. The oscillator's power spec-

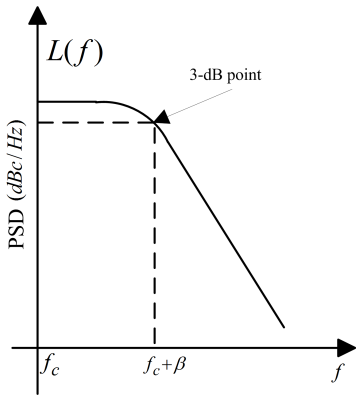

Figure 3.7: Lorentzian power density spectrum (PSD)

trum is usually defined as a single side-band spectrum measured in dBc/Hz (decibels relative to carrier per Hertz) and is given as [11]

$$L(f) = 10\log_{10}\left(\frac{\kappa}{4\pi^2(f_o - f_c)^2 + (\frac{\kappa}{2})^2}\right) \qquad \text{for} \quad 0 \leq f_o \leq \infty \tag{3.14}$$

where f_o is the frequency deviation of the oscillator frequency from the center frequency f_c. The function $L(f)$ in (3.14) exhibits characteristics of a Lorentzian power spectral density function as shown in Figure 3.7. Oscillators are often characterized by the 3-dB linewidth of the PSD spectrum β such that

$$\beta = \frac{\kappa}{4\pi} \tag{3.15}$$

It has been well established that as $t \to \infty$, the phase noise process, $\phi(t)$ can be modelled as a Wiener process with independent Gaussian increments [11]. The variance of the phase noise is thus directly proportional to the 3-dB linewidth, β. For high quality oscillators, β is smaller with less energy dispersion around the desired output frequency.

For discrete time systems, we can model the oscillator phase noise as discrete time Weiner process with independent Gaussian increments, i.e.

$$\begin{aligned}\phi(n+1) &= \sqrt{\kappa}B(n+1) \\ &= \sqrt{\kappa}B(n) + u(n) \\ &= \phi(n) + u(n) \end{aligned} \tag{3.16}$$

where $B(n)$ is the discrete time Brownian motion process with $B(0) = 0$ and $u(n)$ is the Gaussian random variable with $u(n) \in \mathcal{N}(0, 4\pi\beta T_s)$ with T_s being the sampling time interval.

3.4.2 Effects of phase noise in MIMO-OFDM

Considering SISO system, in presence of phase noise, equation (2.8) for the m^{th} OFDM symbol in time domain can be re-written as

$$r_m(n) = e^{j\phi_m(n)} \sum_{l=0}^{L-1} g_m(l) s_m(n-l) + \eta_m(n) \tag{3.17}$$

After FFT processing, the received signal in frequency domain is

$$r_m(k) = \sum_{i=0}^{N-1} \Theta_m(i-k) h_m(i) s_m(i) + \eta_m(k) \tag{3.18}$$

where

$$\Theta_m(i) = \frac{1}{N} \sum_{n=0}^{N-1} e^{j\left(\phi_m(n) - \frac{2\pi(i)n}{N}\right)} \tag{3.19}$$

We can notice from equations (3.17) and (3.18) that the multiplicative effect of phase noise in time domain causes convolution of phase noise with channel and symbols in frequency domain. The phase noise effect on OFDM symbols can be separated

to common phase error (CPE) and inter-carrier interference (ICI) corresponding to $i = k$ and $i \neq k$, respectively, as

$$r_m(k) = \underbrace{\Theta_m(0)}_{CPE} h_m(k) s_m(k) + \underbrace{\zeta_m(k)}_{ICI} + \eta_m(k) \tag{3.20}$$

The CPE and ICI terms can be written as

$$\Theta_m(0) = \frac{1}{N} \sum_{i=0}^{N-1} e^{j\phi_m(n)} \tag{3.21}$$

$$\zeta(k) = \frac{1}{N} \sum_{i=0, i\neq k}^{N-1} \Theta_m(i-k) h_m(i) s_m(i) \tag{3.22}$$

It can be observed that the CPE term is the average of the phase noise process and introduces a common rotation on the received OFDM subcarriers. The ICI term, on the other hand, destroys the orthogonality between the subcarriers. It introduces additive effect resulting from product of channel and transmitted signals from every other subcarriers. The mean energy of the phase noise spectral components depend upon the phase noise linewidth, number of subcarriers and transmitted data rate [12] as

$$E\{\mid \Theta_m(i) \mid^2\} = \frac{1}{N^2} \left\{ 2\Re \left(\frac{b_i^{N+1} - (N+1)b_i + N}{(b_i - 1)^2} \right) - N \right\} \tag{3.23}$$

where b_i can be written as $b_i = e^{j2\pi i/N - \pi\beta R_t}$ and $R_t = N/T_s$ denotes the transmission data rate. The ICI term can be treated as a random Gaussian noise when the channel and transmitted symbols are considered independent and identically distributed complex variables [27]. In [12], the energy of the ICI term is calculated for arbitrary phase noise levels and subcarrier numbers with normalized channel power,

$E\{\mid h_m(k) \mid^2\} = 1$ as

$$
\begin{aligned}
E\{\mid \zeta_m(k) \mid^2\} &= \sigma_s^2 \sum_{i=1}^{N-1} E\{\mid \Theta_m(i) \mid^2\} \\
E\{\mid \zeta_m(k) \mid^2\} &= \frac{\sigma_s^2}{N^2} \sum_{i=1}^{N-1} \left\{ 2\frac{b_i^{N+1} - (N+1)b_i + N}{(b_i - 1)^2} - N \right\} \qquad (3.24)
\end{aligned}
$$

The effect of CPE is dominant when the subcarrier spacing is much higher than the oscillator linewidth ($\beta \ll \Delta f$) but ICI becomes more dominant if the converse is true. CPE can be mitigated by de-rotating the received symbols by the CPE estimate obtained by averaging the phase rotation on known pilot subcarriers in an OFDM symbol [12]. On the other hand, the highly random nature of the ICI makes it very difficult for full phase noise compensation and requires complex algorithms that increases complexity. Hence, the design of the oscillator should be such that β is as low as possible so as to effectively mitigate for the phase noise effects in the digital domain.

Phase noise effects are more severe for oscillators with high β and is very essential to improve oscillator design to maintain low β . For high phase noise levels, ICI power surpasses the signal power and the signal-to-interference plus noise power ratio (SINR) degradation is more than the SNR itself [12] and it is difficult and infeasible to implement phase noise mitigation algorithms. Phase noise can be considered small when the value of βT_s is between 10^{-5} to 10^{-2} such that the mitigation methods are effective. Considering small phase noise with $2\pi\beta T_s \ll 1$, the CPE energy, ICI

energy and SINR can be written as [12]

$$E\{|\ \Theta_m(0)\ |^2\} = 1 - \frac{\pi\beta N}{3R_t} \tag{3.25}$$

$$E\{|\ \zeta_m(k)\ |^2\} = \frac{\pi\beta N\sigma_s^2}{3R_t} \tag{3.26}$$

$$\text{SINR} = \frac{1 - \frac{\pi\beta N}{3R_t}}{\frac{\pi\beta N}{3R_t} + \frac{1}{SNR}} \tag{3.27}$$

where SNR denotes the average signal to noise ratio per subcarrier.

The received signal model as given in (3.20) can be easily extended for MIMO case. The time domain received signal corrupted by phase noise at the q^{th} receiver can then be written from (2.11) and (3.17) as

$$\tilde{\mathbf{r}}_{q,m} = \left[e^{j\phi(0)}, e^{j\phi(1)}, ..., e^{j\phi(N_{tot}+L-1)}\right] \odot \sum_{p=1}^{M_t} \mathbf{h}_{q,p} \star \tilde{\mathbf{s}}_{p,m} + \mathbf{w}_q \tag{3.28}$$

where $e^{j\phi(n)}$ represents one realization of phase noise process for the q^{th} receiver branch and the m^{th} OFDM symbol. Equivalently, the received signal in the frequency domain can be written as

$$\mathbf{r}_m(k) = \sum_{i=0}^{N-1} \mathbf{\Theta}_m(i-k)\mathbf{H}_m(i)\mathbf{s}_m(i) + \boldsymbol{\eta}_m(k) \tag{3.29}$$

where $\mathbf{\Theta}_m(i)$ is the $M_r \times M_r$ diagonal matrix of phase noise frequency domain samples for the i^{th} subcarrier $(i = 0, .., N-1)$ of the m^{th} OFDM symbol. The effect of phase noise for the received symbol can be separated into two terms, the CPE (for $i = k$) and ICI (for $i \neq k$) terms, as

$$\mathbf{r}_m(k) = \underbrace{\mathbf{\Theta}_m(0)}_{CPE}\mathbf{H}_m(k)\mathbf{s}_m(k) + \underbrace{\boldsymbol{\zeta}_m(k)}_{ICI} + \boldsymbol{\eta}_m(k) \tag{3.30}$$

where $\mathbf{r}_m(k)$, $\mathbf{s}_m(k)$, $\boldsymbol{\eta}_m(k)$ and $\boldsymbol{\zeta}_m(k)$ are the $M_r \times 1$ received signal, transmitted signal, ICI and AWGN vectors associated with k^{th} subcarrier of m^{th} OFDM symbol.

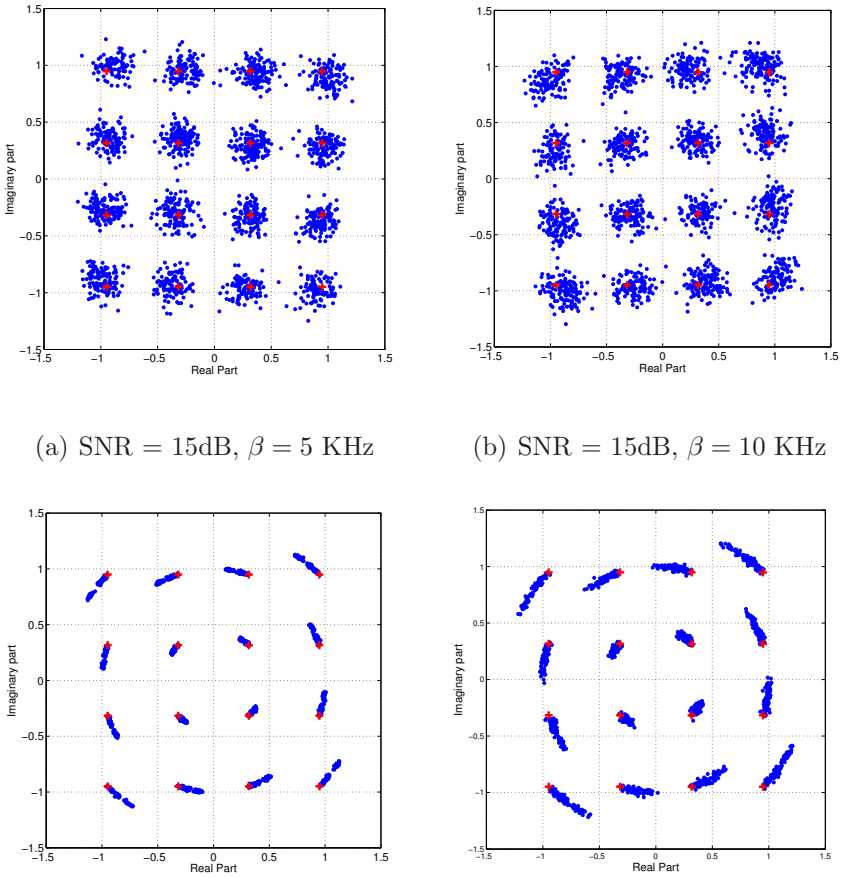

(a) SNR = 15dB, $\beta = 5$ KHz

(b) SNR = 15dB, $\beta = 10$ KHz

(c) SNR = 50dB, $\beta = 5$ KHz

(d) SNR = 50dB, $\beta = 10$ KHz

Figure 3.8: Constellation plot for 16-QAM 2×2 MIMO-OFDM system at different SNR and phase noise linewidth

$\mathbf{H}_m(k)$ is the $M_r \times M_t$ channel matrix and $\mathbf{\Theta}_m(0) = diag\left[\Theta_{m,1}(0), \Theta_{m,2}(0), ..., \Theta_{m,M_r}(0)\right]$ represents the $M_r \times M_r$ diagonal matrix containing CPE terms associated with each receiver branch. Constellation plot for a 2×2 MIMO-OFDM system with different phase noise linewidth at different SNR is shown in Figure 3.8.

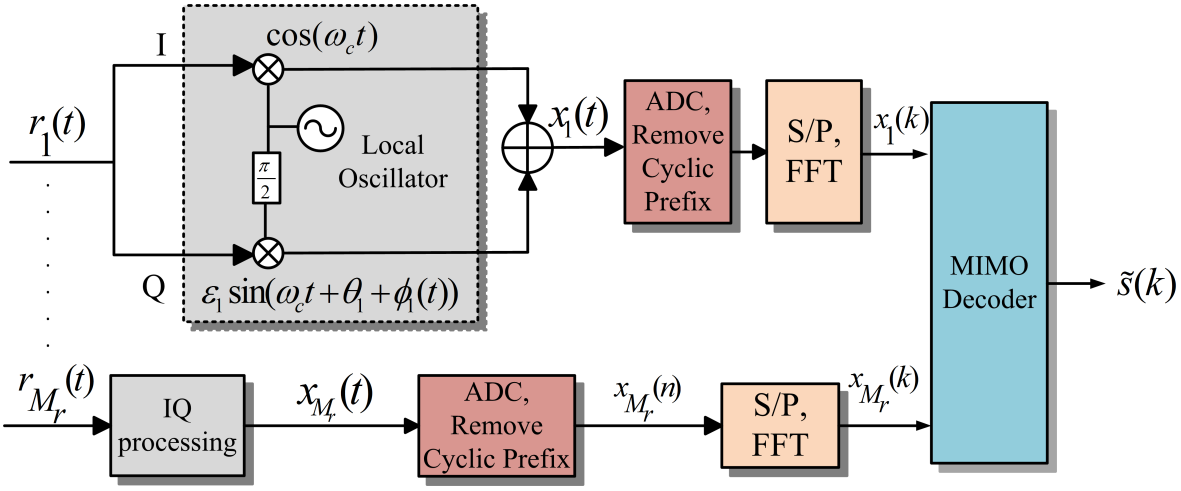

Figure 3.9: MIMO-OFDM receiver suffering from individual IQ-Imbalance and phase noise at each receiver branch.

3.4.3 Joint effects of phase noise and IQ-Imbalance in MIMO-OFDM

Figure 3.9 shows a direct conversion IQ receiver suffering from both IQ-Imbalance and phase noise. The frequency domain received MIMO-OFDM signal suffering from both IQ-Imbalance and phase noise can be obtained by combining (3.30) and (3.10) as

$$\begin{aligned}
\mathbf{x}_m(k) &= \mathbf{K}_1\mathbf{r}_m(k) + \mathbf{K}_2\mathbf{r}_m^{\#}(k) + \boldsymbol{\eta}_m(k) \\
&= \mathbf{K}_1\sum_{i=0}^{N-1}\boldsymbol{\Theta}_m(i-k)\mathbf{H}_m(i)\mathbf{s}_m(i) + \mathbf{K}_2\sum_{i=0}^{N-1}\boldsymbol{\Theta}_m^{\#}(i-k)\mathbf{H}_m^{\#}(i)\mathbf{s}_m^{\#}(i) + \boldsymbol{\eta}_m(k) \\
&= \mathbf{K}_1\boldsymbol{\Theta}_m(0)\mathbf{H}_m(k)\mathbf{s}_m(k) + \mathbf{K}_2\boldsymbol{\Theta}_m^{*}(0)\mathbf{H}_m{}^{\#}(k)\mathbf{s}_m{}^{\#}(k) + \bar{\boldsymbol{\eta}}_m(k) \qquad (3.31)
\end{aligned}$$

where $\bar{\boldsymbol{\eta}}_m(k) = \boldsymbol{\zeta}_m(k) + \boldsymbol{\eta}_m(k)$ represents $M_r \times 1$ ICI plus noise term affecting each receive branch for the m^{th} OFDM symbol at k^{th} subcarrier. The new ICI term, $\boldsymbol{\zeta}_m(k)$,

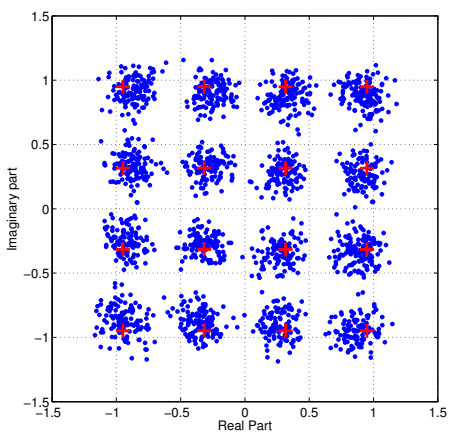

(a) SNR = 15dB, $\{5°, 5\%\}, \beta = 5$ KHz

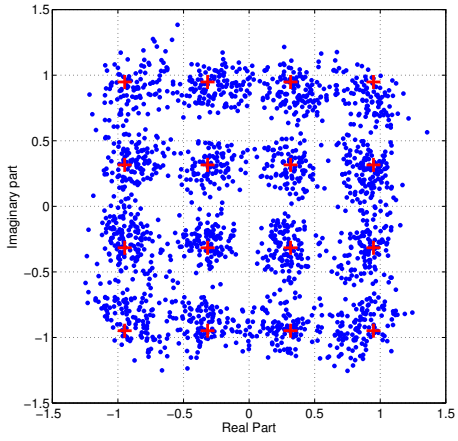

(b) SNR = 15dB, $\{10°, 10\%\}, \beta = 10$ KHz

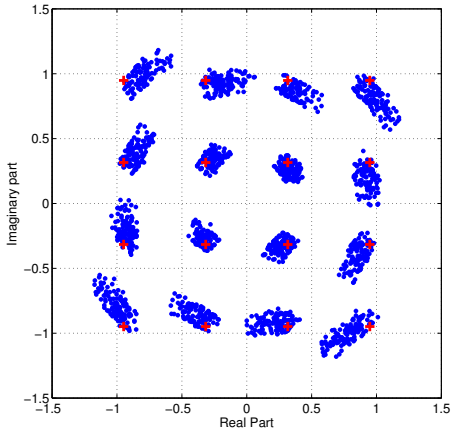

(c) SNR = 50dB, $\{5°, 5\%\}, \beta = 5$ KHz

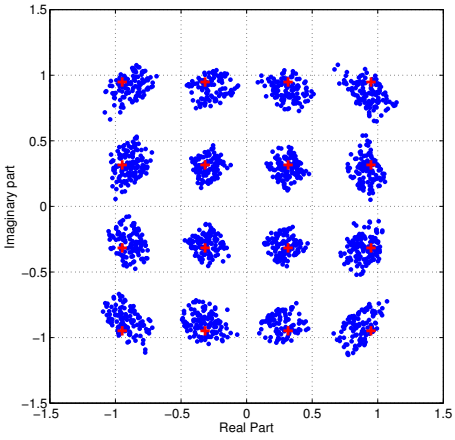

(d) SNR = 50dB, $\{10°, 10\%\}, \beta = 10$ KHz

Figure 3.10: Constellation plot for 16-QAM 2×2 MIMO-OFDM system at different SNR and phase noise linewidth

including both IQ-Imbalance and phase noise can be written as

$$\boldsymbol{\zeta}_m(k) = \mathbf{K}_1 \sum_{i=0, i\neq k}^{N-1} \boldsymbol{\Theta}_m(i-k)\mathbf{H}_m(i)\mathbf{s}_m(i) + \mathbf{K}_2 \sum_{i=0, i\neq -k}^{N-1} \boldsymbol{\Theta}_m^{\#}(i-k)\mathbf{H}_m^{\#}(i)\mathbf{s}_m^{\#}(i) \quad (3.32)$$

The received MIMO-OFDM signal model in (3.31) shows the adverse multiplicative and additive effects of IQ-Imbalance and phase noise. Figure 3.10 shows the con-

stellation diagram of the received 2×2 MIMO-OFDM symbol using 16-QAM under different SNR with different IQ mismatch and phase noise linewidth.

In this chapter, various RF-impairments and their impact on MIMO-OFDM systems were discussed. It can be inferred that in presence of those impairments coupled with noise and channel fading, the performance degradation will be intolerable. In Chapter IV, the techniques to mitigate those impairments and improve system performance is discussed. We first propose the techniques to estimate the impairments then use that information to compensate the adverse effects of impairments at the receiver of MIMO-OFDM systems.

CHAPTER IV

ESTIMATION AND COMPENSATION

4.1 IEEE 802.11a frame format

We consider IEEE 802.11a standard [1] frame format developed for high-speed WLAN (Wi-Fi) that uses OFDM for data transmission. Although developed for SISO systems, it has been used as the building block of its multi-antenna counterpart IEEE 802.11n. Typical parameters of an OFDM symbol based on IEEE 802.11a standard are shown in Table 4.1. The variable transmission data rate can be achieved by choosing appropriate coding rate and modulation format. The available bandwidth of 20 MHz is used by 64 subcarriers that consists of 52 information and 12 null subcarriers (one null subcarrier centered at DC). Pilots and null subcarriers are used to fine tune the channel estimation at receiver and to prevent ICI, respectively. Furthermore, to reduce the ISI, a cyclic prefix of 16 OFDM subcarriers is appended at the beginning of the OFDM symbol before transmission.

One OFDM frame consists of several OFDM symbols. The data transmission stage is preceded by transmission of several training symbols collectively known as preamble (see Figure 4.1). The preamble symbols are generally divided into short training (ST) and long training (LT) symbols. The ST symbols are generally used

Table 4.1: IEEE 802.11a parameters [1]

Parameter	Value
Modulation Format	BPSK, QPSK, 16/64-QAM
Coding	Convolutional with rate $1/2, 2/3, 3/4$
Bandwidth	20 MHz
Subcarrier spacing	320 KHz
Symbol Duration	$4\mu s$
Cyclic Prefix Length	$800ns$
Number of subcarriers	64
Number of data subcarriers	48
Number of pilot subcarriers	4

for detection of signals, gain control and diversity selection. In each ST symbol, 12 subcarriers are QPSK modulated and the rest 52 subcarriers are null subcarriers. For LT symbols, 52 subcarriers are BPSK modulated that are used for channel estimation and synchronization. The signal (SIG) field is transmitted after LT symbols that is used to transmit modulation format and coding rate information for data subcarriers. For MIMO systems, this also contains multi-antenna configuration information. After SIG field, OFDM data symbols are transmitted that contain 4 pilot subcarriers, 48 modulated data subcarriers and 16 null subcarriers. Although these parameters are already standardized for IEEE 802.11a, modifications of the preamble and data

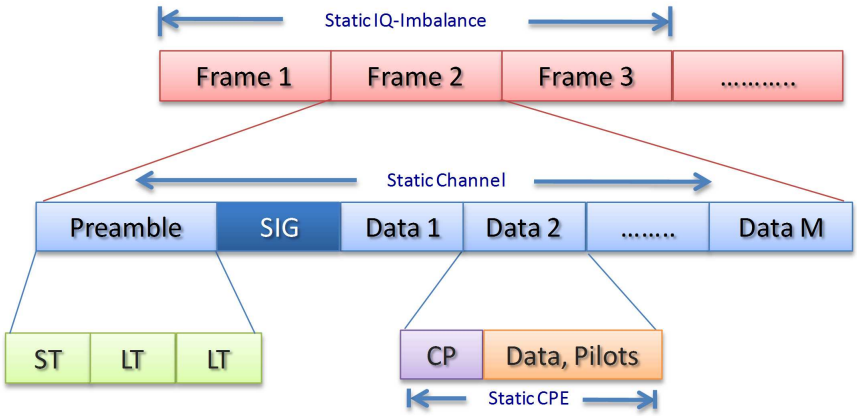

Figure 4.1: IEEE 802.11a OFDM frame structure

symbol structures can be made according to system requirements.

4.2 Preamble design

In packet or non-packet OFDM based standards, OFDM symbols contain known pilot signals. Packet based OFDM transmission standards such as 802.11a/n usually consider full pilot OFDM training symbols at preamble stage. OFDM data symbols also consist of several scattered pilot signals within the OFDM symbol. In non-packet based OFDM standards such as in mobile-LTE or mobile-WiMAX systems, preamble might or might not be present depending upon the system requirements but scattered pilot signals are always present within an OFDM data symbol.

For coherent detection of OFDM symbols, estimation of channel from each transmit to receive branch is necessary. LT OFDM symbols are used for coarse channel estimation at the receiver in a typical fixed OFDM system. In MIMO systems,

it is necessary that the design of preamble be such that the channel can be uniquely identified between any transmit-receive pair. Considering a MIMO-OFDM system that transmits two full $N \times 1$ training OFDM symbols from each of the M_t transmit branches, the received frequency domain LT symbols at M_r receive branches can be written as,

$$\mathbf{R}_T = \mathbf{H}_T \mathbf{S}_T + \mathbf{N}_T \tag{4.1}$$

where $\mathbf{R}_T = [\mathbf{r}_{r1} \;\; \mathbf{r}_{r2}]$ is the $NM_r \times 2$ received training symbol matrix, $\mathbf{H}$ is the $NM_r \times NM_t$ channel matrix, $\mathbf{S}_T = [\mathbf{s}_{t1} \;\; \mathbf{s}_{t2}]$ is the $NM_t \times 2$ transmitted training symbol matrix and $\mathbf{N}_T$ is the $NM_r \times 2$ AWGN component. The estimate of channel can then be obtained by using the least squares (LS) estimation method using the pseudo-inverse of $\mathbf{S}_T$ as,

$$\hat{\mathbf{H}}_T = \mathbf{R}_T \mathbf{S}_T^{\dagger} = \mathbf{H}_T + \mathbf{N}_T \mathbf{S}_T^{\dagger} \tag{4.2}$$

where $\hat{\mathbf{H}}_T$ is the estimated $NM_r \times NM_t$ channel matrix and $\mathbf{S}_T^{\dagger}$ is the pseudo-inverse of the transmitted training symbol matrix.

For MIMO-OFDM systems, in order to detect the channel between any transmit-receive antenna pair, the optimal design condition for preamble symbol is that it should possess orthogonality and shift-orthogonality for at least the channel length [57, 48]. This condition is to minimize the channel estimation error. Based on this condition and using 802.11a frame format, four types of LT symbols can be constructed [58] that achieve orthogonality and shift-orthogonality in time and frequency domain. They are time multiplexed (TM), time orthogonal (TO), subcarrier multi-

Table 4.2: Preamble structures and required overhead

Preamble Structure	Overhead(No. of OFDM symbols)
TM	$2M_t$
TO	$2M_t$
SM	2
SO	2

plexed (SM) and subcarrier orthogonal structures [58]. The preamble structures for MIMO-OFDM system employing 2 transmit antennas are shown in Figure 4.2. The details of estimating the channel and the corresponding derivation of mean squared error (MSE) is given in [58, 7]. The overhead associated with those four types of preamble structures are shown in Table 4.2. From Table 4.2, it can be seen that for TM and TO structures, the number of training symbols required is always twice the number of transmit antennas. On the other hand, it remains fixed for SM and SO structures. Also, for TM and TO structures, the channel estimates are available for all the subcarriers while for SM and SO structures, channel estimates for only selected subcarriers are available. The design of the preamble structure in the presence of IQ-Imbalance and phase noise for MIMO-OFDM systems has the following requirements:

- The preamble should possess orthogonality and shift orthogonality for detection of MIMO symbols.

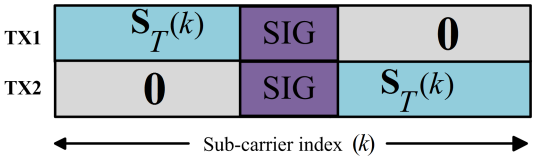

(a) Time-multiplexed preamble structure

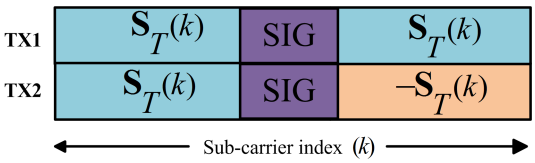

(b) Time-orthogonal preamble structure

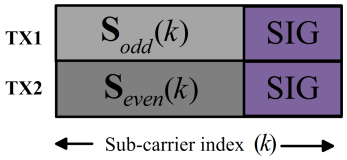

(c) Subcarrier-multiplexed preamble structure

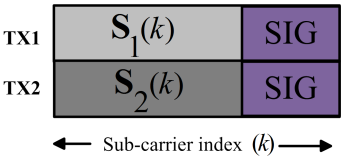

(d) Subcarrier-orthogonal preamble structure

Figure 4.2: Different preamble structures for MIMO-OFDM system based on IEEE 802.11a standard [1]

- Since the CPE term is dynamic, on a symbol by symbol basis, using more OFDM symbols in preamble results in considerable estimation error [42].
- The received signal contains data from mirror subcarriers due to IQ-Imbalance. Hence, the preamble should be designed such that the effect of mirror subcarriers is eliminated.

Based on the these requirements, SM preamble is the best choice which we consider in this thesis. It requires only two LT preamble symbols to estimate the IQ-Imbalance parameters. Also, the estimates will be minimally affected by changing phase noise

per OFDM symbol. We define matrices $\mathbf{T}_1$ and $\mathbf{T}_2$ that contain M_t training symbol vectors of size $N \times 1$ to be transmitted from M_t transmit antennas as

$$\mathbf{T}_1 = \{\boldsymbol{\gamma} \circ \boldsymbol{\xi}_1, \boldsymbol{\gamma} \circ \boldsymbol{\xi}_2, ..., \boldsymbol{\gamma} \circ \boldsymbol{\xi}_{M_t}\} \tag{4.3}$$

$$\mathbf{T}_2 = \{\boldsymbol{\gamma} \circ \boldsymbol{\xi}_1^{'}, \boldsymbol{\gamma} \circ \boldsymbol{\xi}_2^{'}, ..., \boldsymbol{\gamma} \circ \boldsymbol{\xi}_{M_t}^{'}\} \tag{4.4}$$

where γ is a $N \times 1$ vector of known training symbol that can be optimized according to the system requirements and the $N \times 1$ vectors $\boldsymbol{\xi}_p$ and $\boldsymbol{\xi}_p^{'}$, corresponding to p^{th} transmit antenna, are given as

$$\boldsymbol{\xi}_p(k) = \Pi_{p-1}\{[1, \mathbf{0}_{M_t-1}, 1, \mathbf{0}_{M_t-1}, ..., 1, \mathbf{0}_{M_t-1}]\}^T \tag{4.5}$$

$$\boldsymbol{\xi}_p^{'}(k) = \begin{cases} -\boldsymbol{\xi}_p(k) & \text{for } k \in \left\{1, 2, .., \frac{N}{2} - 1\right\} \\ \boldsymbol{\xi}_p(k) & \text{for } k \in \left\{-\frac{N}{2}, -\frac{N}{2} + 1, .., -1\right\} \end{cases} \tag{4.6}$$

In (4.5), Π_{p-1} represents the cyclic shift operation over $p-1$ samples and $\mathbf{0}_{M_t-1}$ denotes an all-zero vector. Fig. 4.3 shows the preamble structure for the special case of 2 transmit antennas. With the above proposed preamble structure and without considering ICI and noise, the received signal vector for the two consecutive training symbols can be written as

$$\boldsymbol{\psi}_1(k) = \mathbf{K}_1\hat{\mathbf{H}}_{pre}(k)\mathbf{t}_1(k) + \mathbf{K}_2\hat{\mathbf{H}}_{pre}^{\#}(k)\mathbf{t}_1^{\#}(k) \tag{4.7}$$

$$\boldsymbol{\psi}_2(k) = \mathbf{K}_1(\hat{\mathbf{H}}_{pre}(k) + \boldsymbol{\delta})\mathbf{t}_2(k) - \mathbf{K}_2(\hat{\mathbf{H}}_{pre}^{\#}(k) + \boldsymbol{\delta}^*)\mathbf{t}_2^{\#}(k) \tag{4.8}$$

where $\mathbf{t}_1(k)$ and $\mathbf{t}_2(k)$ are the k^{th} row of $\mathbf{T_1}$ and $\mathbf{T_2}$ with each of them containing only one non-zero element $\lambda_1(k)$ and $\lambda_2(k)$ respectively. $\hat{\mathbf{H}}_{pre}(k) = \boldsymbol{\Theta}_{pre}(0)\mathbf{H}(k)$ and $\hat{\mathbf{H}}_{pre}^{\#}(k) = \boldsymbol{\Theta}_{pre}^{*}(0)\mathbf{H}^{\#}(k)$ represent the effective channel matrix at the k^{th} and $-k^{th}$

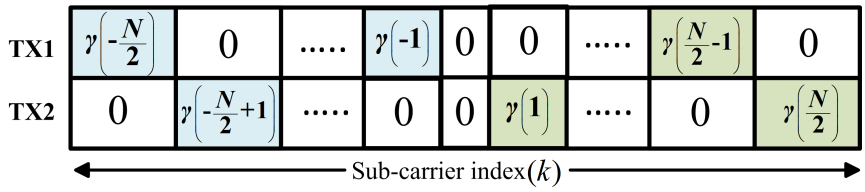

(a) First OFDM Training Symbol

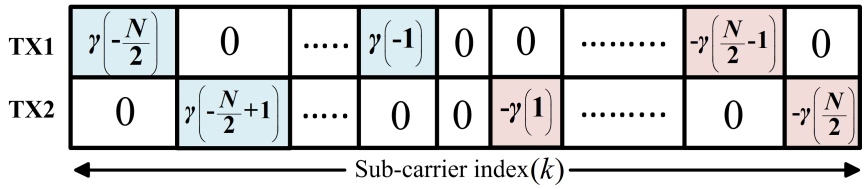

(b) Second OFDM Training Symbol

Figure 4.3: OFDM preamble structure for 2 transmit antennas.

subcarriers with $\boldsymbol{\Theta}_{pre}(0)$ being the CPE associated with the training symbols. $\boldsymbol{\delta}$ is the $M_r \times 1$ vector representing error term due to different CPEs affecting two consecutive training symbols. This error term is the same for all the subcarriers due to the same CPE effect on every subcarrier.

4.3 Effective channel estimation

Since the CPE term is the same for all the subcarriers, it is sufficient to estimate the effective channel at the preamble stage. We define two vectors, $\boldsymbol{\chi}_a(k)$ and $\boldsymbol{\chi}_b(k)$ as

$$\boldsymbol{\chi}_a(k) = \{\boldsymbol{\psi}_1(k) + \boldsymbol{\psi}_2(k)\}/2\lambda_1(k) = \mathbf{K}_1\hat{\mathbf{h}}_p(k) + \boldsymbol{\rho} \tag{4.9}$$

$$\boldsymbol{\chi}_b(k) = \{\boldsymbol{\psi}_1(k) - \boldsymbol{\psi}_2(k)\}/2\lambda_2^*(k) = \mathbf{K}_2\hat{\mathbf{h}}_p^{\#}(k) - \boldsymbol{\rho} \tag{4.10}$$

where $\hat{\mathbf{h}}_p(k) = \boldsymbol{\Theta}_{pre}(0)\mathbf{h}_p(k)$ and $\hat{\mathbf{h}}_p^{\#}(k) = \boldsymbol{\Theta}_{pre}^*(0)\mathbf{h}_p^{\#}(k)$ represent the p^{th} column vector of $\hat{\mathbf{H}}_{pre}(k)$ and $\hat{\mathbf{H}}_{pre}^{\#}(k)$, respectively and $\boldsymbol{\rho} = (\mathbf{K}_1\boldsymbol{\delta} - \mathbf{K}_2\boldsymbol{\delta}^*)/2$. Using (4.9), (4.10) and the fact that $\mathbf{K}_2 = \mathbf{I}_{M_r} - \mathbf{K}_1^*$, we define $M_r \times 1$ vector $\mathbf{e}(k)$ as,

$$\mathbf{e}(k) = \boldsymbol{\chi}_a(k) + \boldsymbol{\chi}_b^{\#}(k) = \hat{\mathbf{h}}_p(k) + \boldsymbol{\rho} - \boldsymbol{\rho}^* \tag{4.11}$$

From (4.11), the channel vector corresponding to the k^{th} subcarrier ($k = kM_t + p, k = 0, 1, ..., [N/M_t]$) of the p^{th} receiver branch is estimated with very small error, $\boldsymbol{\rho} - \boldsymbol{\rho}^* = \frac{1}{2}(\boldsymbol{\delta} - \boldsymbol{\delta}^*)$, that does not depend on the IQ-imbalance parameters and is solely due to CPE difference between two consecutive long training symbols. Hence, we take the estimated channel vector $\hat{\mathbf{h}}_p(k) \approx \mathbf{e}(k)$. After all the channel estimates are obtained, the estimation can be improved further by employing a linear minimum mean squared error (LMMSE) scheme when the correlation between the subcarriers and average SNR is known [59]. The LMMSE channel estimate can be calculated as [59],

$$\hat{\mathbf{h}}_{p,q}^{\mathrm{LMMSE}} = \mathbf{R}_{hh}\left(\mathbf{R}_{hh} + \frac{\varrho}{\mathrm{SNR}}\mathbf{I}_N\right)^{-1}\hat{\mathbf{h}}_{p,q} \tag{4.12}$$

where $\hat{\mathbf{h}}_{p,q}^{\mathrm{LS}}$ is the $(N/M_t) \times 1$ estimated channel vector at the preamble stage for each $p^{th} - q^{th}$ transmit-receive pair. $\mathbf{R}_{hh} = \mathbb{E}\left\{\mathbf{h}_{p,q}\mathbf{h}_{p,q}^H\right\}$ is the autocorrelation matrix of the channel elements in the frequency domain. $\varrho = \mathbb{E}\{|s_k|^2\}\,\mathbb{E}\{|1/s_k|^2\}$ is a constant which is fixed for any given modulation format (e.g. for 16-QAM, $\varrho = 17/9$ [59]). To reduce the high complexity introduced by this estimation method, a low-rank approximation method is also introduced in [59]. The channel vectors for the rest of the subcarriers can be estimated using interpolation along the subcarriers or

by employing iterative transform domain techniques [60, 61] which are summarized below.

4.3.1 Channel estimation using interpolation

To obtain a full channel matrix associated with each subcarrier for coherent detection, different interpolation techniques can be used based on the complexity requirements of the system. Considering a simple linear interpolation method, the channel at the k^{th} subcarrier for the p^{th} and q^{th} transmit and receive pair for a 2×2 MIMO system can be written as,

$$\hat{h}_{pre,p,q}(k) = \frac{\hat{h}_{pre,p,q}(k-1) + \hat{h}_{pre,p,q}(k+1)}{2} \tag{4.13}$$

The channel associated with the edge subcarriers can be estimated by extrapolation, but, the estimation error due to extrapolation is comparatively large and causes loss in system performance. To reduce this, the subcarriers at the edge of the OFDM frequency spectrum can be modulated with lower order modulation for better detection or can be discarded completely. The number of subcarriers which can be discarded is low for low order MIMO systems but increases with more number of transmit antennas. In terms of complexity, interpolation amongst subcarriers is the best choice since it is simplest to implement.

4.3.2 Channel estimation using transform domain techniques

This method of channel estimation for OFDM transmission provides more accurate estimation than interpolation methods when the channel estimates are not available

for all subcarriers [62]. It uses the limited available channel estimates obtained at preamble stage to estimate the channel for all subcarriers. Since only N/M_t channel estimates are available for any transmit/receive branch, this method iteratively reconstructs the missing channel estimates by employing successive FFT/IFFT transformations. Let $\hat{\mathbf{h}}_{k_0}$ where $k_0 = 0, 1, .., (N/M_t) - 1$ be the frequency domain effective channel estimates obtained using training symbols at preamble for any $p-q$ transmit-receive pair.

1. Perform zero padding at those subcarrier indices where the channel is not defined. This will extend the length of effective channel estimates, $\hat{\mathbf{h}}_{k_0}$, from N/M_t to N. Lets consider the extended zero-padded channel to be $\hat{\mathbf{h}}_{k_1}$.

2. For iteration i, transform $\hat{\mathbf{h}}_{k_1}$ into time domain by using an N point IFFT i.e., $\hat{\mathbf{h}}_{n_i} = \boldsymbol{\mathcal{F}}_N^{-1}\left\{\hat{\mathbf{h}}_{k_1}\right\}$.

3. Apply a rectangular window $w(n)$ to select L significant channel taps from $\hat{\mathbf{h}}_{n_i}$. The rectangular window can be defined as

$$\begin{aligned} w(n) &= 1 \qquad \text{for} \qquad (N-L)/2 \leq n \leq (N+L)/2 \\ &= 0 \qquad \text{otherwise} \end{aligned} \tag{4.14}$$

   where $n = 0, .., N-1$

4. Transform the windowed time domain channel response, $\hat{\mathbf{h}}_{n_i}$, to frequency domain using N point FFT. Let this channel response be $\hat{\mathbf{h}}_{k_i}$.

5. Substitute the known N/M_t channel estimates from $\hat{\mathbf{h}}_{k_0}$ into $\hat{\mathbf{h}}_{k_i}$.

6. Calculate the mean squared error, MSE $= \mathbb{E}\left\{|\hat{\mathbf{h}}_{k_0} - \hat{\mathbf{h}}_{k_i}|^2\right\}$ for $\{k_0, k_i\} = 0, 1, .., (N/M_t) - 1$.

7. Repeat steps 2-6 to meet the desired accuracy.

The knowledge of channel length and the location of the most significant channel tap is the main requirement for this procedure. In practice, the most significant tap will be the one with the highest magnitude. The algorithm also works better when the window length matches with the true channel length. The channel response for all other transmit-receive pairs can be estimated by the same method and the overall channel response for each subcarrier can then be estimated.

4.4 IQ-Imbalance parameter estimation

The estimation of phase and amplitude imbalances due to IQ-imbalance is necessary to mitigate the effects of IQ-Imbalance. To estimate the IQ-imbalance parameters at the preamble stage using (4.9 - 4.11), for $k = 0, ..., N-2$, we define

$$\begin{aligned} \boldsymbol{\alpha}(k) &= \mathbf{e}(k) - \mathbf{e}(k+1) \\ &= \hat{\mathbf{h}}_p(k) - \hat{\mathbf{h}}_{p+1}(k+1) \qquad (4.15) \\ \boldsymbol{\beta}(k) &= \boldsymbol{\chi}_a(k) - \boldsymbol{\chi}_a(k+1) \\ &= \mathbf{K}_1\hat{\mathbf{h}}_p(k) - \mathbf{K}_1\hat{\mathbf{h}}_{p+1}(k+1) \\ &= \mathbf{K}_1\boldsymbol{\alpha}(k) \qquad (4.16) \end{aligned}$$

where $\boldsymbol{\chi}_a(k)$ and $\mathbf{e}(k)$ are defined in 4.9 and 4.11 respectively. The phase and amplitude imbalance parameters are then calculated as

$$\tilde{\boldsymbol{\theta}}(k) = -\arg\{2(\boldsymbol{\beta}(k) \oslash \boldsymbol{\alpha}(k)) - \mathbf{1}_{M_r}\} \tag{4.17}$$

$$\tilde{\boldsymbol{\varepsilon}}(k) = \text{abs}\{2(\boldsymbol{\beta}(k) \oslash \boldsymbol{\alpha}(k)) - \mathbf{1}_{M_r}\} \tag{4.18}$$

where $\mathbf{1}_{M_r}$ is the $M_r \times 1$ all one vector and $\oslash$ represents element-wise division operation. It can be noticed that the estimates of imbalance parameters are totally independent of the different CPE term for two consecutive long training symbols. The obtained imbalance parameters can be averaged over all subcarriers to get a better estimate. To further increase the accuracy of the estimates and because of the slow varying nature of IQ-imbalance parameters, these parameters can be averaged over several OFDM blocks.

4.5 Effective channel tracking and data detection

Since we typically assume quasi-static channel for WLAN and Wi-Fi systems, the channel response can be considered fixed within an OFDM frame. The channel estimation obtained at the preamble would have been sufficient for several OFDM symbols, but, since CPE changes from one OFDM symbol to another, it needs to be compensated on a per symbol basis. Assuming there are r pilot subcarriers in m^{th} OFDM symbol from j^{th} transmit branch with pilot values $d_{m,j}(1)$, $d_{m,j}(2)$, ..., $d_{m,j}(r)$, it is possible to update the effective channel matrix estimates obtained from (4.11) at data transmission stage for efficient phase noise mitigation and data detection.

The $M_r \times 1$ received pilot signals at l^{th} and $-l^{th}$ subcarrier of the m^{th} OFDM symbol where $l \in 1, 2, .., r$ can be written as (without considering ICI and noise)

$$\mathbf{x}_m(l) = \mathbf{K}_1 \boldsymbol{\Upsilon}_m \mathbf{y}_m(l) + \mathbf{K}_2 \boldsymbol{\Upsilon}^*_m \mathbf{y}^{\#}_m(l) \tag{4.19}$$

$$\mathbf{x}^{\#}_m(l) = \mathbf{K}^*_1 \boldsymbol{\Upsilon}^*_m \mathbf{y}^{\#}_m(l) + \mathbf{K}^*_2 \boldsymbol{\Upsilon}_m \mathbf{y}_m(l) \tag{4.20}$$

where the diagonal matrix $\boldsymbol{\Upsilon}_m$,

$$\boldsymbol{\Upsilon}_m = \begin{bmatrix} \Upsilon_{m,1} & 0 & \cdots & 0 \\ 0 & \Upsilon_{m,2} & \cdots & 0 \\ \vdots & \vdots & \ddots & \vdots \\ 0 & 0 & \cdots & \Upsilon_{m,M_r} \end{bmatrix} \tag{4.21}$$

represents the updating parameters to compensate varying phase error for each receiver branch such that $\Upsilon_{m,q} = \Theta_{m,q}(0)/\Theta_{pre,q}(0)$. $\mathbf{K}_1 = diag(k^{(1)}_1, .., k^{(1)}_{M_r})$ and $\mathbf{K}_2 = diag(k^{(2)}_1, .., k^{(2)}_{M_r})$ are the IQ-imbalance matrices. We also define vector $\mathbf{y}_m(l)$ as $\mathbf{y}_m(l) = \{y_{m,1}(l), .., y_{m,M_r}(l)\}^T$ such that $\mathbf{y}_m(l) = \hat{\mathbf{H}}_{pre}(l)\mathbf{d}_m(l)$ where $\hat{\mathbf{H}}_{pre}(l)$ is the estimated channel matrix and $\mathbf{d}_m(l) = \{d_{m,1}(l), .., d_{m,M_t}(l)\}^T$ is the vector of transmitted pilots from different transmitter branch at l^{th} subcarrier.

Algorithm 1 summarizes the procedure to compute the updating parameter matrix to compensate for varying CPE for each OFDM symbol. As the CPE is fixed for all the subcarriers, it is possible to get a better estimate of the updating matrix by averaging it out over all pilot subcarriers. After finding the updating matrix, the transmitted data vector at the k^{th} subcarrier, $\tilde{\mathbf{s}}_m(k)$, can be estimated using

Algorithm 1 Calculation of updating parameter matrix $\boldsymbol{\Upsilon}_m$

Input $\rightarrow \hat{\mathbf{K}}_1, \hat{\mathbf{K}}_2, \hat{\mathbf{H}}_{pre}(k), \boldsymbol{\Psi}, r, \mathbf{x}_m(l), \mathbf{x}_m^{\#}(l)$

Output $\rightarrow \boldsymbol{\Upsilon}_m$

- Initialize $\rightarrow q = 1$

  while $q \leq M_r$ **do**

  - Set $\mathbf{X}_{1,q} = \begin{bmatrix} k_q^{(1)} & k_q^{(1)} \\ k_q^{*(2)} & k_q^{*(2)} \end{bmatrix}$, $\mathbf{X}_{2,q} = \begin{bmatrix} k_q^{(1)} & -k_q^{(1)} \\ k_q^{*(2)} & -k_q^{*(2)} \end{bmatrix}$

    * Initialize $\rightarrow l = 1$

      while $l \leq r$ **do**

      1. Set $\boldsymbol{z}_q(l) = [x_{m,q}(l), x_{m,q}^{\#}(l)]^T$
      2. Compute $y_{m,q}(l)$ and $y_{m,q}^{\#}(l)$
      3. Compute $\hat{\mathbf{C}}_q(l) = y_{m,q}(l)\mathbf{X}_{1,q} + y_{m,q}^{\#}(l)\mathbf{X}_{2,q}$
      4. Compute $\mathbf{Q}_q(l) = (\hat{\mathbf{C}}_q^H(l)\hat{\mathbf{C}}_q(l) + \Psi_{q,q}\mathbf{I}_2)^{-1}\hat{\mathbf{C}}_q^H(l)$
      5. Compute $\hat{\boldsymbol{\varphi}}_q(l) = \mathbf{Q}_q(l)\mathbf{z}_q(l)$
      6. $l = l + 1$

  - Compute $\hat{\boldsymbol{\varphi}}_q = \frac{1}{r}\sum_{l=1}^{r}\hat{\boldsymbol{\varphi}}_q(l)$
  - Compute $\Upsilon_{m,q} = \hat{\varphi}_q(1) + j\hat{\varphi}_q(2)$
  - $q = q + 1$

- Set $\boldsymbol{\Upsilon}_m = diag\{\Upsilon_{m,q}\}_{q=1}^{M_r}$

$\hat{\mathbf{H}}_m(k) = \boldsymbol{\Upsilon}_m\hat{\mathbf{H}}_{pre}(k)$, $\hat{\mathbf{K}}_1$, $\hat{\mathbf{K}}_2$ and solving

$$\min\|\hat{\mathbf{s}}_m(k) - \mathbf{A}(k)\hat{\mathbf{x}}_m(k)\|^2 \tag{4.22}$$

where $\hat{\mathbf{s}}_m(k) = \{\tilde{\mathbf{s}}_m(k), \tilde{\mathbf{s}}_m^{\#}(k)\}^T$ and $\hat{\mathbf{x}}_m(k) = \{\mathbf{x}_m(k), \mathbf{x}_m^{\#}(k)\}^T$ are the estimated

and received signal vectors, respectively. For zero forcing (ZF) and minimum mean squared error (MMSE) based receivers

$$\mathbf{A}_{\mathrm{ZF}}(k) = (\mathbf{W}^H(k)\mathbf{W}(k))^{-1}\mathbf{W}^H(k) \tag{4.23}$$

$$\mathbf{A}_{\mathrm{MMSE}}(k) = (\mathbf{W}^H(k)\mathbf{W}(k) + \mathbf{R})^{-1}\mathbf{W}(k)^H \tag{4.24}$$

where,

$$\mathbf{W}(k) = \begin{bmatrix} \hat{\mathbf{K}}_1\hat{\mathbf{H}}_m(k) & \hat{\mathbf{K}}_2\hat{\mathbf{H}}_m^{\#}(k) \\ \hat{\mathbf{K}}_2^{*}\hat{\mathbf{H}}_m(k) & \hat{\mathbf{K}}_1^{*}\hat{\mathbf{H}}_m^{\#}(k) \end{bmatrix} \tag{4.25}$$

and $\mathbf{R} = \mathbf{\Psi}\otimes\mathbf{I}_{M_r}$ is the noise + ICI power that can be estimated from null-subcarriers. For N OFDM short symbols with N_{null} null subcarriers, this correlation matrix $\mathbf{\Psi}$ can be estimated as [40]

$$\mathbf{\Psi} = \frac{1}{LN_{null}}\sum_{l=1}^{L}\sum_{k=1}^{N_{null}}\mathbf{x}_l(k)\mathbf{x}_l^H(k) \tag{4.26}$$

In Chapter V, the efficiency of the estimation and compensation techniques proposed in this chapter to mitigate RF-impairments will be verified by simulation. The following chapter presents various simulation results in terms of mean squared error (MSE) and bit-error rate (BER) for the performance evaluation under different scenarios.

CHAPTER V

PERFORMANCE RESULTS

5.1 Simulation setup

To analyse the system performance, Monte-Carlo simulation [63] to obtain mean-squared error and bit error rate under various scenarios is performed in MATLAB. OFDM symbol format is based on IEEE 802.11a standard for fixed-WLAN systems [1]. A summary of the used parameters can also be found in Table 4.1. At the beginning of transmission, two full pilot OFDM preamble symbols are generated using binary phase shift keying (BPSK) modulation. The pilot symbols to be inserted in OFDM data symbols are generated using quadrature phase shift keying (QPSK) modulation format. For each transmit branch, the data are generated as random bit streams which are grouped and mapped into a suitable modulation format (4/16/64 QAM).

The wireless channel is modelled as a 7-tap multipath Rayleigh fading channel with exponential power delay profile. The channel is assumed to be independent for each transmit-receive pair [52]. Furthermore, AWGN with zero mean and unit variance is added to the received signal at the receiver. Independent oscillators are assumed at each receive branch with independent IQ-Imbalance and phase noise. IQ-

Imbalance parameters are chosen in accordance to realistic practical values ranging between 1%-10% in amplitude and 1°-5° in phase. The phase noise process is modelled as a discrete Brownian motion process with independent Gaussian increments as given in Chapter III.

The OFDM transmission process consists of transmission of preamble symbols followed by OFDM data symbols on a frame by frame basis. One OFDM frame consists of 50 OFDM symbols excluding the preamble. In OFDM preamble symbols, out of 64 available subcarriers in one OFDM symbol, 52 subcarriers are modulated to be used as training symbols and 11 subcarriers at each edge of the OFDM spectrum and one at DC are left as null subcarriers. For OFDM data symbol, 48 subcarriers are used as data, 4 as pilots and 12 subcarriers are null subcarriers. Data and pilots are mapped into subcarriers of an OFDM symbol and fed into 64-point IFFT block. The resulting time domain symbols are converted to a serial data stream and the last 16 time domain OFDM samples are appended at the beginning of the OFDM symbol as cyclic prefix. The data stream is mapped over the antenna using spatial multiplexing [64] and then passed through the channel.

At each receive branch, independent IQ-Imbalance and phase noise is added to the received OFDM time domain samples. After FFT operation, the preamble symbols are used to estimate the effective channel and IQ-Imbalance parameters. Those parameters along with the pilot symbols in OFDM data symbol are used to track the effective channel according to the algorithm discussed in Chapter IV. After all the parameters are estimated, the receiver then applies minimum mean squared

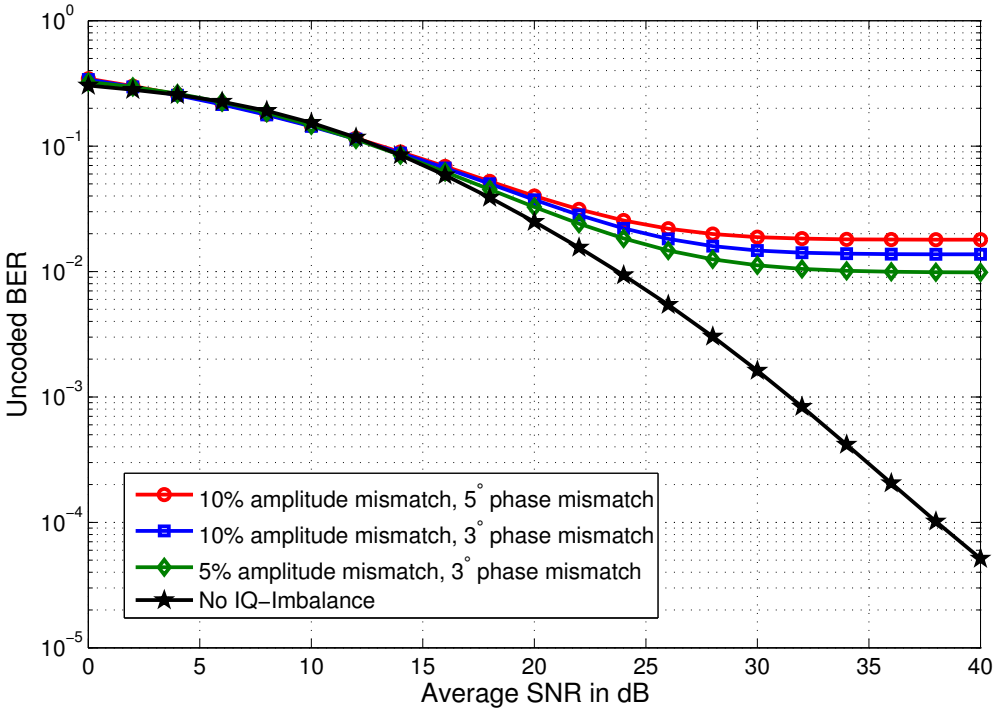

Figure 5.1: BER performance of an uncoded 16-QAM, 2×2 MIMO-OFDM system with different IQ-Imbalances

error (MMSE) based decoding scheme on a per-subcarrier basis [65] to estimate the transmitted frequency domain signals at each subcarrier.

5.2 Effect of IQ-Imbalance and phase noise in MIMO-OFDM systems

The effect of impairments in MIMO-OFDM system is analyzed using BER simulation. The effect of the impairments is simulated by assuming that the receiver has perfect channel knowledge but lacks IQ-Imbalance and phase noise information. In Figure 5.1, the effect of IQ-Imbalance on the performance of spatial multiplexing in a 2×2

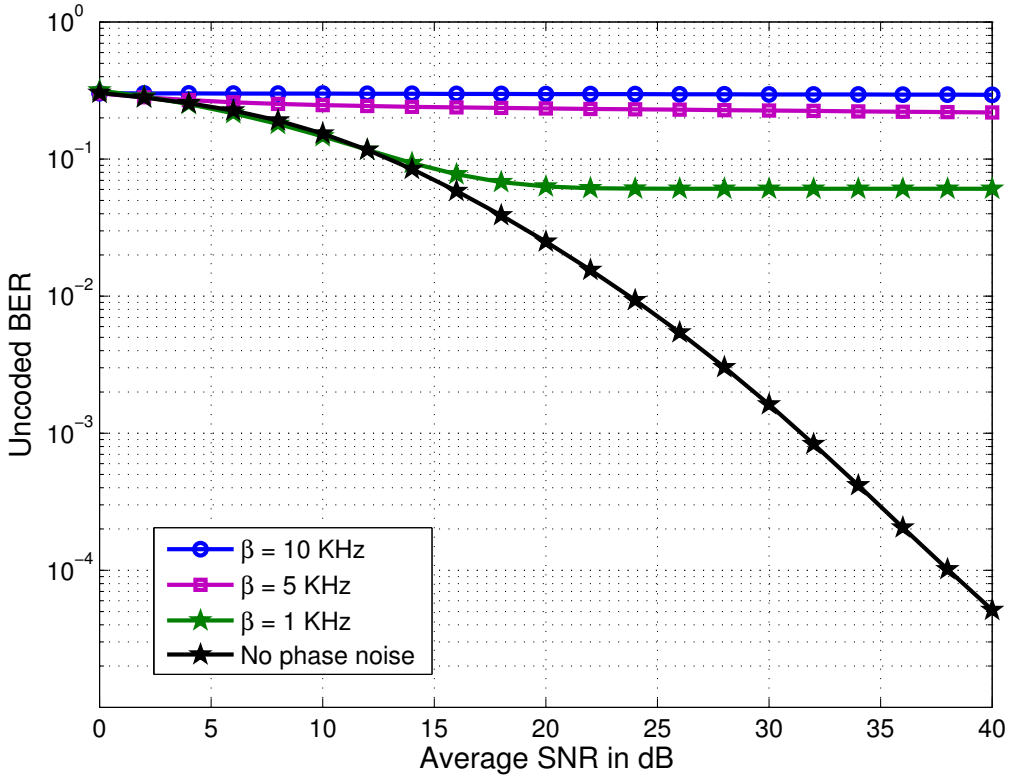

Figure 5.2: BER performance of an uncoded 16-QAM, 2×2 MIMO-OFDM system at various phase noise linewidth

MIMO-OFDM system using 16-QAM modulation is shown. It can be seen that even very small phase and amplitude mismatch causes significant performance degradation. Similarly, the effect of phase noise is depicted in Figure 5.2 for 2×2 MIMO-OFDM system using 16-QAM modulation with different phase noise linewidth. It can be seen that the phase noise also has a severe effect on system performance.

The joint effect of IQ-Imbalance and phase noise is shown in Figure 5.3 for a 2×2 MIMO-OFDM system using 16-QAM modulation. Different IQ-Imbalance

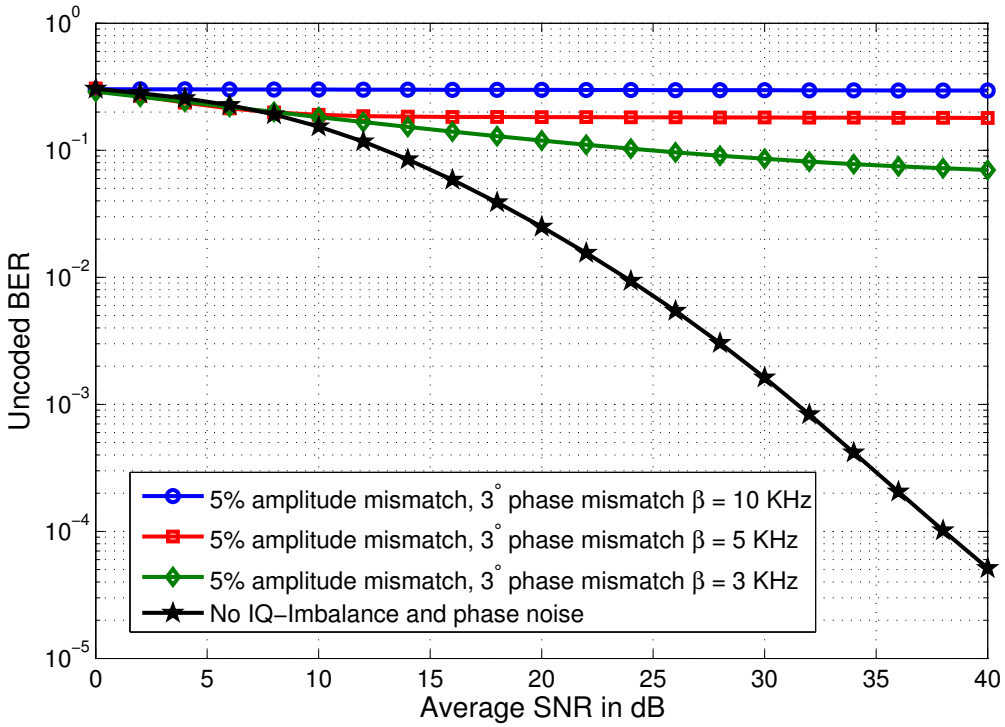

Figure 5.3: BER performance of an uncoded 16-QAM, 2×2 MIMO-OFDM system with both IQ-Imbalance and phase noise

values and phase noise linewidth are taken for simulation. As expected, the joint effects of these impairments cause significant performance loss in terms of BER that is higher than the individual effects of those impairments.

5.3 Mean-squared error

The estimation of effective channel and IQ-Imbalance parameters using preamble symbols at the beginning of the OFDM frame transmission is analyzed using mean

squared error metric given as

$$\mathrm{MSE}_{\mathbf{H}} = \mathbb{E}\left\{\|\hat{\mathbf{H}}_m - \tilde{\mathbf{H}}_m\|^2\right\} \tag{5.1}$$

where $\hat{\mathbf{H}}_m$ represents the actual effective channel containing the CPE term and $\tilde{\mathbf{H}}_m$ is the effective channel estimated by using the tracking algorithm. The MSE in channel estimation is averaged over several OFDM frames and all transmit-receive pairs. Similarly, the MSE metric for IQ-Imbalance parameter estimation can be given as

$$\mathrm{MSE}_{\hat{\mathbf{K}}_1} = \mathbb{E}\left\{\|\tilde{\mathbf{K}}_1 - \mathbf{K}_1\|^2\right\} \tag{5.2}$$

Figure 5.4 shows the MSE in channel estimation for 2×2 and 4×4 MIMO-OFDM systems using an interpolation technique to estimate the overall channel. Fixed IQ-Imbalance of (5°,10%) is applied at each receive branch with variable phase noise linewidth, β. We can see that for higher β, the MSE is also higher which can be explained by the fact that the ICI power increases with increasing β. The flooring effect is due to the error propagation from the initial channel estimation errors.

The MSE for channel estimation using transform domain iterative techniques with 40 iterations with IQ-Imbalance of (5°,10%) and phase noise linewidth $\beta = 5$ KHz at each receive branch is shown in Figure 5.5. We can see that this method improves the system performance as compared to interpolation method especially for a 4×4 MIMO system where lesser channel estimates are available at preamble stage. For higher phase noise linewidth, β, this scheme also has degrading performance due to increased ICI power from phase noise.

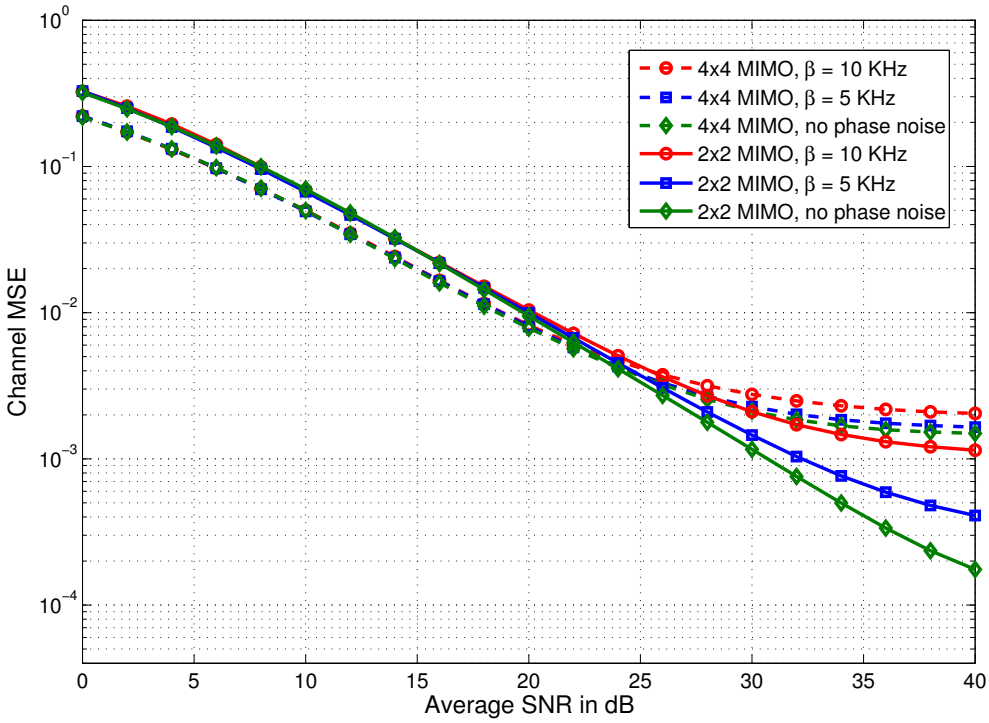

Figure 5.4: Channel MSE for 2×2 and 4×4 MIMO-OFDM using interpolation technique. IQ-Imbalance of (5°,10%) is applied at each receive branch

In Figure 5.6, a comparison of interpolation and transform domain channel estimation techniques is shown for a 4×4 MIMO-OFDM system with IQ-Imbalance of (5°,10%) and phase noise linewidth, $\beta = 5$ KHz. It can be observed that with higher number of transmit-receive pairs, transform domain technique with sufficient iterations has superior performance than interpolation technique.

The accuracy of IQ-Imbalance parameters estimation can be analyzed using MSE of matrix $\mathbf{K}_1$ that contains all the phase and amplitude mismatches at all the receive branches. In Figure 5.7, the MSE of IQ-Imbalance parameters for a 4×4

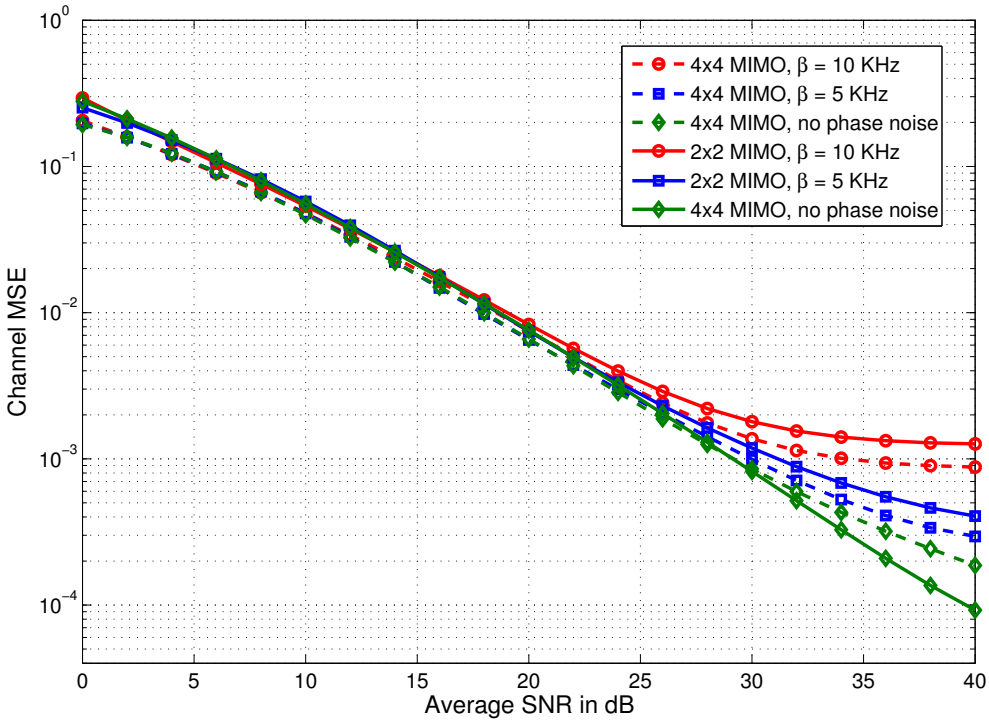

Figure 5.5: Channel MSE for 2×2 and 4×4 MIMO-OFDM with iterative transform domain technique. IQ-Imbalance of (5°,10%) is applied at each receive branch

MIMO system is depicted. Similar results are obtained for a 2×2 MIMO system. As seen, the proposed estimation method performs very well at high phase noise linewidth, β. Also, at low SNR where AWGN is dominant, it can be seen that the phase noise level does not have significant effect on MSE. At high SNRs, however, ICI becomes dominant and causes performance loss that is dependent upon the phase noise linewidth.

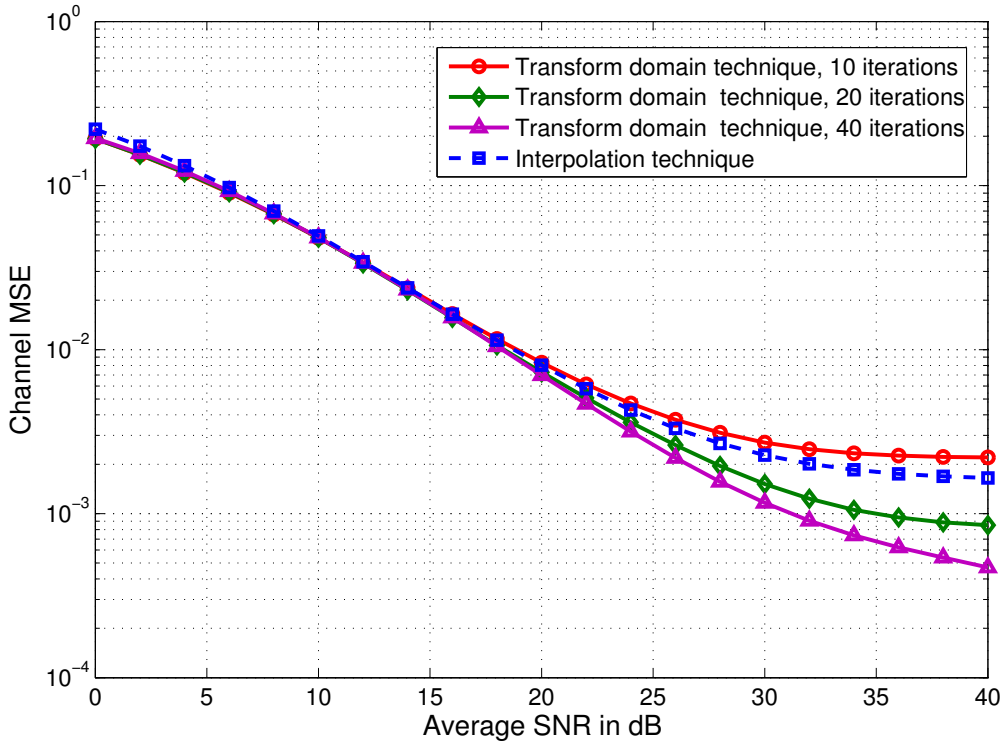

Figure 5.6: Comparison of channel estimation techniques for a 4×4 MIMO system with IQ-Imbalance of (5°,10%) and $\beta = 5$ KHz at each receive branch

5.4 Bit error rate

In this section, the performance of the proposed estimation and tracking scheme for detection of transmitted frequency domain OFDM symbols is demonstrated. The estimated OFDM symbols are de-mapped and the corresponding bit stream is generated. It is then compared with the transmitted bits and error bits are found out that gives the bit error rate at a particular SNR.

In Figures 5.8 and 5.9, the BER results for 2×2 and 4×4 MIMO-OFDM systems using 16-QAM is depicted. We can see that the compensation of only IQ-

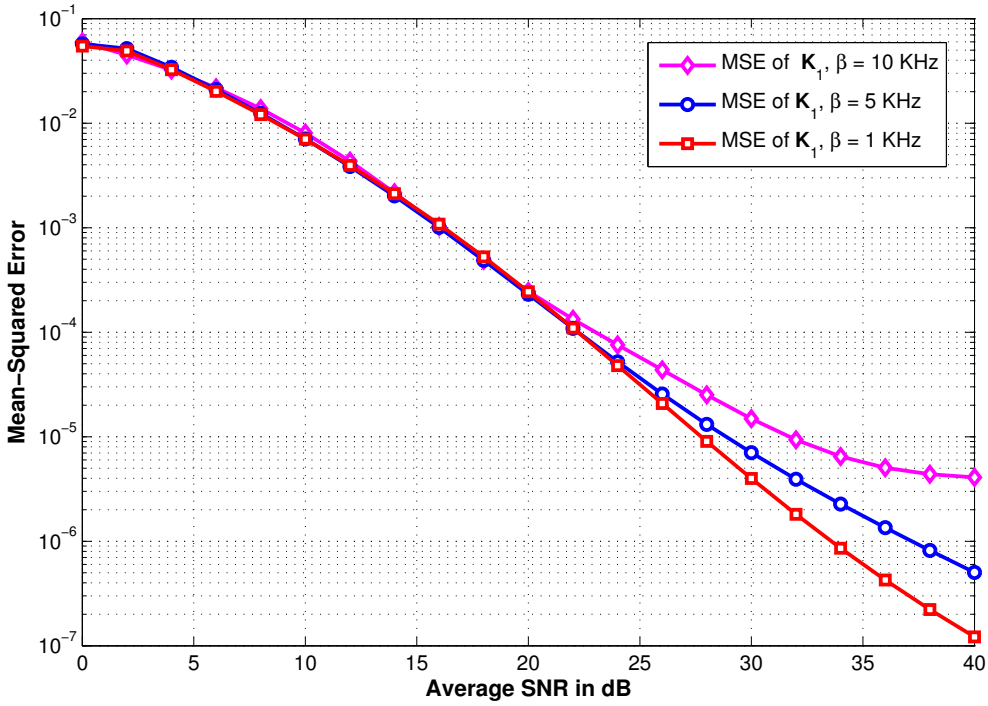

Figure 5.7: MSE in estimation of $\mathbf{K}_1$ for 4×4 MIMO system at various phase noise linewidth, β

Imbalance or phase noise does not improve the system performance. Hence, both the impairments should be compensated to get acceptable system performance. Furthermore, it is evident from the results that iterative transform domain channel estimation technique provides better performance for 4×4 MIMO than 2×2 MIMO system. At BER of 10^{-2}, the gain provided by iterative transform domain technique for 4×4 MIMO against interpolation technique is around 8dB while it is only 1 dB for 2×2 MIMO. It is due to the fact that the iterative technique can re-construct the channel more effectively with less channel estimates than interpolation technique which is

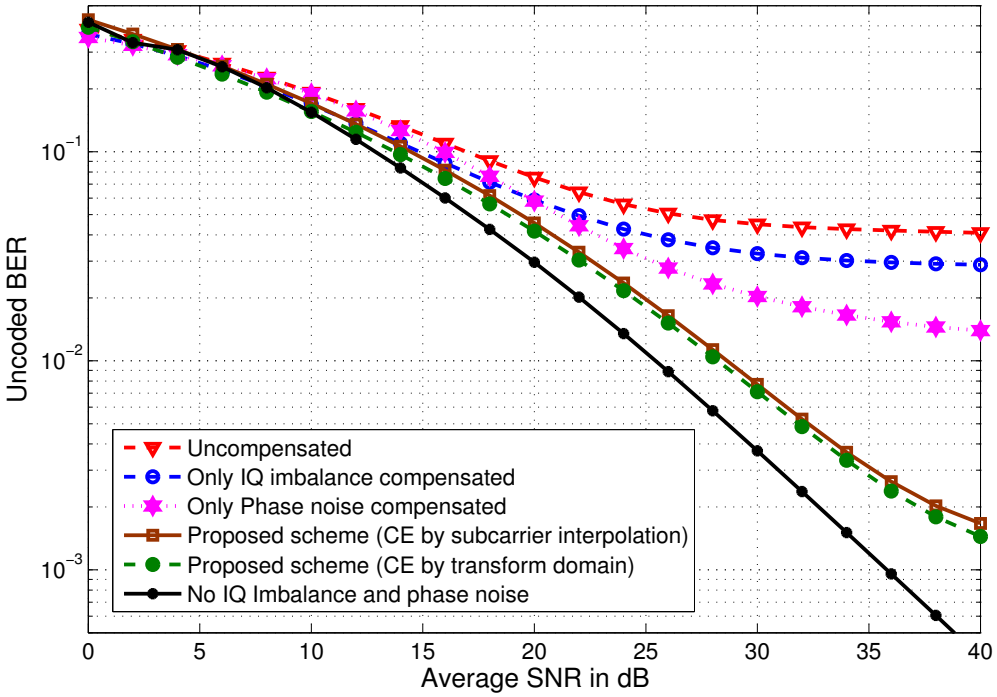

Figure 5.8: BER performance of an uncoded 16-QAM, 2x2 MIMO-OFDM system for $\beta = 5$ KHz and IQ-Imbalance of (5°,10%) at each receiver branch

also evident from MSE results in the previous section. The results for 2×2 MIMO-OFDM with 4-QAM modulation and iterative channel estimation is also shown in Figure 5.10 where we can see similar performance enhancement when the proposed scheme is applied.

5.5 Complexity analysis

The complexity of the proposed estimation and tracking scheme is analyzed by calculating the number of floating point operations per second (FLOPS) required for its

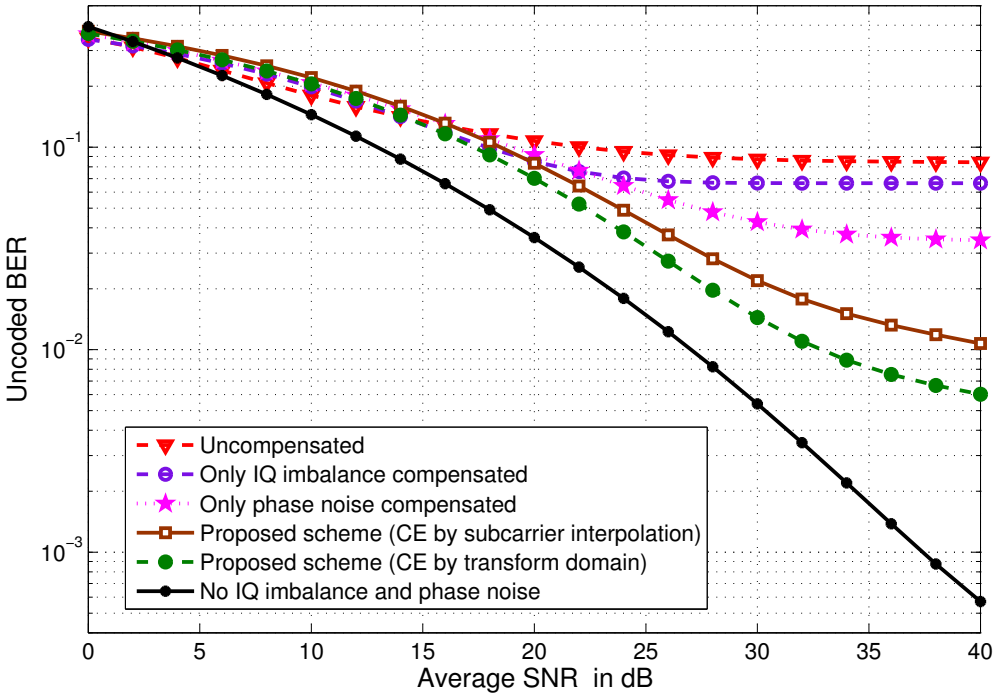

Figure 5.9: BER performance of an uncoded 16-QAM, 4x4 MIMO-OFDM system for $\beta = 5$ KHz and IQ-Imbalance of (5°,10%) at each receiver branch

implementation. For channel and IQ-Imbalance parameters estimation, flops required to calculate (4.9), (4.10), (4.11), (4.15), (4.16), (4.17) and (4.18) are derived. The results are shown in Table 5.1.

For a 2×2 MIMO-OFDM system using 64 subcarriers with 52 data subcarriers the number of flops required to estimate channel and IQ-Imbalance parameters is 3952. The complexity analysis for overall channel estimation using interpolation or transform domain iterative techniques is not included in this calculation. Since transform domain iterative techniques are more complex to implement, a suitable method

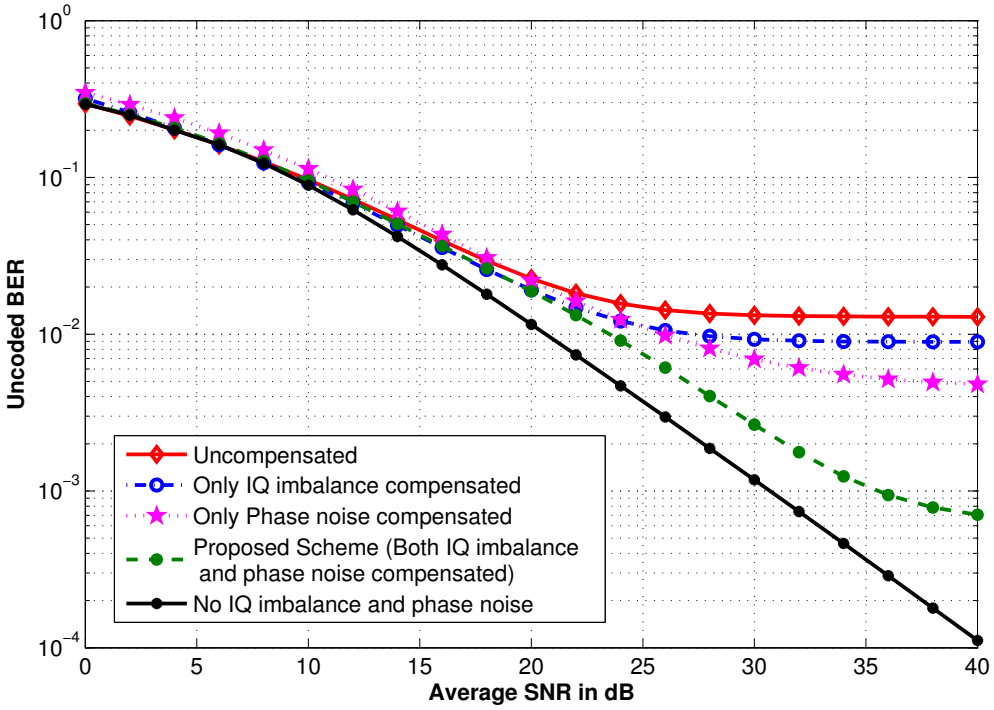

Figure 5.10: BER performance of an uncoded 4-QAM, 2×2 MIMO-OFDM system for $\beta = 5$ KHz and IQ-Imbalance of (5°,10%) at each receiver branch

should be chosen for overall channel estimation based on the system requirements.

Next, we calculate the complexity of the effective channel tracking algorithm (Algorithm 1) as given in Chapter IV. The results are given in Table 5.2. The calculation of total number of flops also includes the $M_r(2r + 4)$ flops required to average the updating parameter over pilot subcarriers for each receive antenna. The complexity to implement the effective channel tracking algorithm when calculated for a 2×2 MIMO-OFDM system with 4 pilot subcarriers is 2104.

The proposed estimation and tracking scheme can be compared with the one

Table 5.1: Computational Complexity of proposed effective channel and IQ-Imbalance parameters estimation technique in terms of number of flops required

Operation	Number of flops required
Channel estimation, equation (4.9)	$N(8M_r + 2)$
Channel estimation, equation (4.10)	$N(8M_r + 2)$
Channel estimation, equation (4.11)	$2NM_r$
IQ-Imbalance parameters estimation, equation (4.15)	$2NM_r$
IQ-Imbalance parameters estimation, equation (4.16)	$2NM_r$
IQ-Imbalance parameters estimation, equation (4.17)	$14NM_r$
Total flops required	$N(36M_r + 4)$

Table 5.2: Computational complexity of proposed tracking method (Algorithm 1) in terms of number of flops required

Operation	Number of flops required
Algorithm 1, step 2	$12M_tM_r$
Algorithm 1, step 3	$56rM_r$
Algorithm 1, step 4	$140rM_r$
Algorithm 1, step 5	$24rM_r$
Total flops required	$M_r((12M_t + 238)r + 4)$

given in [45] in terms of the number of complex additions and multiplications required. The channel estimation in (4.9)-(4.11) only requires $3N$ complex additions

and $2N$ complex multiplications. Also, the IQ-imbalance parameters estimation in (4.15)-(4.18) requires $2N$ complex additions and $2N$ complex multiplications. The estimation process does not involve any matrix inversion. The tracking algorithm involves inversion of a 2×2 matrix for rM_r times. It also involves extra $13rM_r$ complex multiplications and $4rM_r$ complex additions. The scheme proposed in [45] is more complex than our proposed scheme since it involves higher number of complex multiplications. Note that in [45], the analysis is done only for SISO systems while the computational complexity increases exponentially with the number of transmit/receive antennas.

In this chapter, the performance of the proposed estimation and effective channel tracking method is evaluated through simulation. It is observed that the proposed scheme performs well in terms of MSE and BER for different MIMO configurations and impairment parameters. Furthermore, the complexity in implementation of the scheme is also derived in terms of number of flops required. In Chapter VI, concluding remarks and possible future work including the important aspects and findings of this thesis will be discussed.

CHAPTER VI

CONCLUSIONS

6.1 Summary of the thesis

In this thesis, a joint estimation and compensation scheme to mitigate IQ-Imbalance and phase noise with channel estimation in MIMO-OFDM systems was presented. As a starting point, signal, channel and RF impairments modelling were discussed. The impact of RF impairments on the performance of MIMO-OFDM systems was demonstrated through signal model and constellation diagrams. It was pointed out that constellation rotation and ICI are the major impacts of IQ-Imbalance and phase noise. It was also observed that severe performance loss occurred in the presence of those impairments in OFDM systems while the loss was even more pronounced in MIMO-OFDM systems. The need to mitigate those impairments in a joint fashion was pointed out and was also the central point of this thesis.

For MIMO-OFDM systems based on IEEE 802.11 a/n standard, a suitable preamble structure was introduced to estimate the initial channel and IQ-Imbalance. As CPE changes from one OFDM symbol to another, the effective channel estimate obtained at the preamble stage is not suitable for subsequent OFDM symbols in an OFDM frame. Hence, using pilot symbols in data stage of OFDM transmission, a

method to update the effective channel estimates by updating the CPE was discussed. An algorithm was presented that could find the updating parameters corresponding to each receive branch. Using ZF and MMSE schemes, it was shown that the effective channel estimates together with IQ-Imbalance parameters can then be used to efficiently detect the transmitted data. The performance of the proposed scheme for spatial multiplexing in MIMO-OFDM systems was verified through simulation and it was shown that it provides significant performance improvement in terms of BER. The complexity associated with implementation of the estimation and tracking procedure was also calculated based on the number of flops required.

6.2 Future work

The proposed compensation technique in this thesis can be further improved to build more robust MIMO-OFDM transceivers. For instance, joint compensation of several RF impairments can be considered including DC-offset, even-order distortion, non-linearities etc. As those unavoidable impairments are always present in wireless transceivers, methods to jointly estimate and mitigate those impairments are highly desired. Another extension that can be applied is the elimination of the quasi-static channel assumption. In this thesis, it is assumed that the wireless channel between any transmit-receive antenna pair remains constant for several OFDM symbols. However, for mobile wireless systems, this assumption is no longer valid and the channel needs to be estimated for each OFDM symbol.

An assumption is also made in this thesis that the impairments are present only at the receiver. Joint compensation techniques that also consider transmitter side impairments can increase the reliability of a MIMO-OFDM system which is also a possible extension of this thesis. An equivalent received signal model can be formulated that includes both transmitter and receiver impairments, however, it is sometimes preferred to compensate at transmitter and receiver separately.

It is further assumed that the IQ-Imbalance parameters are frequency independent and are constant for the entire bandwidth. However, in [7], it is pointed out that wireless transceivers might also suffer from frequency dependent IQ-Imbalances due to high carrier frequency and mobility of wireless systems. A more realistic IQ-Imbalance model that considers both frequency dependent and frequency independent IQ-Imbalance can be used to come up with new estimation and compensation schemes.

Among the two degrading effects introduced by phase noise, CPE and ICI, the main focus of this thesis was to estimate and mitigate the CPE which has more destructive effect as compared to ICI. However, to completely mitigate phase noise, ICI term should also be considered and methods to estimate and compensate the ICI can be developed for more robust communication systems with some added complexity.

BIBLIOGRAPHY

[1] Supplement to IEEE standard for information technology - telecommunications and information exchange between systems - local and metropolitan area networks - specific requirements. part 11: wireless LAN medium access control (MAC) and physical layer (PHY) specifications: high-speed physical layer in the 5 GHz band. *IEEE Std 802.11a-1999*, 1999.

[2] I. Emre Telatar. Capacity of multi-antenna Gaussian channels. *European Transactions on Telecommunications*, 10:585–595, 1999.

[3] K. Fazel and S. Kaiser. *Multi-Carrier and Spread Spectrum Systems*. John Wiley & Sons, Inc., New York, NY, USA, 2003.

[4] H. Yang. A road to future broadband wireless access: MIMO-OFDM-Based air interface. *IEEE Communications Magazine*, 43(1):53 –60, 2005.

[5] M. Jiang and L. Hanzo. Multiuser MIMO-OFDM for next-generation wireless systems. *IEEE Proceedings*, 95(7):1430 –1469, 2007.

[6] G. Fettweis, M. Lohning, D. Petrovic, M. Windisch, P. Zillmann, and W. Rave. Dirty RF: a new paradigm. In *IEEE 16th International Symposium on Personal, Indoor and Mobile Radio Communications*, volume 4, pages 2347 –2355 Vol. 4, 2005.

[7] T. Schenk. *RF imperfections in high-rate wireless systems: impact and digital compensation*. Springer Publishing Company, Incorporated, 1st edition, 2008.

[8] R.M. Rao and B. Daneshrad. Analog impairments in MIMO-OFDM systems. *IEEE Transactions on Wireless Communications*, 5(12):3382 –3387, 2006.

[9] B. Razavi. *RF microelectronics*. Prentice-Hall, Inc., Upper Saddle River, NJ, USA, 1998.

[10] A. Tarighat, R. Bagheri, and A.H. Sayed. Compensation schemes and performance analysis of IQ imbalances in OFDM receivers. *IEEE Transactions on Signal Processing*, 53(8):3257 – 3268, 2005.

[11] A. Demir, A. Mehrotra, and J. Roychowdhury. Phase noise in oscillators: a unifying theory and numerical methods for characterization. *IEEE Transactions on Circuits and Systems I: Fundamental Theory and Applications*, 47(5):655 – 674, May 2000.

[12] S. Wu and Y. Bar-Ness. OFDM systems in the presence of phase noise: consequences and solutions. *IEEE Transactions on Communications*, 52(11):1988 – 1996, 2004.

[13] A.A. Abidi. Direct-conversion radio transceivers for digital communications. In *IEEE International Solid-State Circuits Conference*, pages 186 –187, 363–4, February 1995.

[14] S. Mirabbasi and K. Martin. Classical and modern receiver architectures. *IEEE Communications Magazine*, 38(11):132 – 139, November 2000.

[15] B. Razavi. Design considerations for direct-conversion receivers. *IEEE Transactions on Circuits and Systems II: Analog and Digital Signal Processing*, 44(6):428 –435, June 1997.

[16] M. Valkama, M. Renfors, and V. Koivunen. Advanced methods for I/Q imbalance compensation in communication receivers. *IEEE Transactions on Signal Processing*, 49(10):2335 –2344, October 2001.

[17] A. Schuchert, R. Hasholzner, and P. Antoine. A novel IQ imbalance compensation scheme for the reception of OFDM signals. *IEEE Transactions on Consumer Electronics*, 47(3):313 –318, August 2001.

[18] K.-Yu Sung and C. chao Chao. Estimation and compensation of I/Q imbalance in OFDM direct-conversion receivers. *IEEE Journal of Selected Topics in Signal Processing*, 3(3):438 –453, 2009.

[19] J.C. Oostveen, A. Schoonen, and F. Willems. Baseband compensation of transmitter and receiver IQ imbalance for OFDM in frequency selective fading channels. In *IEEE 7th Workshop on Signal Processing Advances in Wireless Communications*, pages 1 –5, 2006.

[20] A. Tarighat and A.H. Sayed. MIMO OFDM Receivers for Systems With IQ Imbalances. *IEEE Transactions on Signal Processing*, 53(9):3583 – 3596, 2005.

[21] T.C.W. Schenk, P.F.M. Smulders, and E.R. Fledderus. Estimation and compensation of TX and RX IQ imbalance in OFDM-based MIMO systems. In *IEEE Radio and Wireless Symposium*, pages 215 – 218, 2006.

[22] H. Kamata, K. Sakaguchi, and K. Araki. An effective IQ imbalance compensation scheme for MIMO-OFDM communication system. In *IEEE 16th International Symposium on Personal, Indoor and Mobile Radio Communications*, volume 1, pages 181 –185, 2005.

[23] Y. Zou, M. Valkama, and M. Renfors. Performance analysis of space-time coded MIMO-OFDM systems under I/Q imbalance. In *IEEE International Conference on Acoustics, Speech and Signal Processing*, volume 3, pages III–341 –III–344, 2007.

[24] Y. Zou, M. Valkama, and M. Renfors. Digital Compensation of I/Q Imbalance Effects in Space-Time Coded Transmit Diversity Systems. *IEEE Transactions on Signal Processing*, 56(6):2496 –2508, 2008.

[25] A. Demir, A. Mehrotra, and J. Roychowdhury. Phase noise and timing jitter in oscillators. In *Proceedings of the IEEE Custom Integrated Circuits Conference*, pages 45 –48, May 1998.

[26] R. Corvaja and S. Pupolin. Phase noise spectral limits in OFDM systems. *Wireless Personal Communications*, 36:229–244, 2006. 10.1007/s11277-006-0476-x.

[27] A. Garcia Armada. Understanding the effects of phase noise in orthogonal frequency division multiplexing (OFDM). *IEEE Transactions on Broadcasting*, 47(2):153 –159, June 2001.

[28] L. Piazzo and P. Mandarini. Analysis of phase noise effects in OFDM modems. *IEEE Transactions on Communications*, 50(10):1696 – 1705, October 2002.

[29] T. Pollet, M. Van Bladel, and M. Moeneclaey. BER sensitivity of OFDM systems to carrier frequency offset and Wiener phase noise. *IEEE Transactions on Communications*, 43(234):191 –193, 1995.

[30] P. Robertson and S. Kaiser. Analysis of the effects of phase-noise in orthogonal frequency division multiplex (OFDM) systems. In *IEEE International Conference on Communications, Seattle, 'Gateway to Globalization'.*, volume 3, pages 1652 –1657 vol.3, June 1995.

[31] V. Syrjala, M. Valkama, N.N. Tchamov, and J. Rinne. Phase noise modelling and mitigation techniques in ofdm communications systems. In *Wireless Telecommunications Symposium,*, pages 1 –7, 2009.

[32] F. Munier, T. Eriksson, and A. Svensson. An ICI reduction scheme for OFDM system with phase noise over fading channels. *IEEE Transactions on Communications*, 56(7):1119 –1126, 2008.

[33] D. Petrovic, W. Rave, and G. Fettweis. Common phase error due to phase noise in OFDM-estimation and suppression. In *15th IEEE International Symposium on Personal, Indoor and Mobile Radio Communications*, volume 3, pages 1901 – 1905 Vol.3, 2004.

[34] D. Petrovic, W. Rave, and G. Fettweis. Intercarrier interference due to phase noise in OFDM - estimation and suppression. In *IEEE 60th Vehicular Technology Conference*, volume 3, pages 2191 – 2195, 2004.

[35] H.-G. Ryu, Y. Li, and J.-S. Park. An improved ICI reduction method in OFDM communication system. *IEEE Transactions on Broadcasting*, 51(3):395 – 400, 2005.

[36] R. Corvaja and A.G. Armada. SINR degradation in MIMO-OFDM systems with channel estimation errors and partial phase noise compensation. *IEEE Transactions on Communications*, 58(8):2199 –2203, 2010.

[37] T.C.W. Schenk, X.-Jiao Tao, P.F.M. Smulders, and E.R. Fledderus. Influence and suppression of phase noise in multi-antenna OFDM. In *IEEE 60th Vehicular Technology Conference*, volume 2, pages 1443 – 1447 Vol. 2, 2004.

[38] S. Bittner, E. Zimmermann, and G. Fettweis. Exploiting phase noise properties in the design of MIMO-OFDM receivers. In *IEEE Wireless Communications and Networking Conference*, pages 940 –945, 312008-april3 2008.

[39] P. Liu and Y. Bar-Ness. Phase noise mitigation for V-BLAST OFDM system. In *IEEE International Symposium on Microwave, Antenna, Propagation and EMC Technologies for Wireless Communications*, volume 2, pages 1194 – 1197 Vol. 2, 2005.

[40] P. Liu, S. Wu, and Y. Bar-Ness. A phase noise mitigation scheme for MIMO WLANs with spatially correlated and imperfectly estimated channels. *IEEE Communications Letters*, 10(3):141 – 143, March 2006.

[41] P. Rabiei, W. Namgoong, and N. Al-Dhahir. Efficient pilot-aided digital baseband compensation of phase noise ICI in OFDM receivers. In *IEEE Global Telecommunications Conference*, pages 1 –5, 302009-dec.4 2009.

[42] S. Bittner, E. Zimmermann, and G. Fettweis. Iterative phase noise mitigation in MIMO-OFDM systems with pilot aided channel estimation. In *IEEE 66th Vehicular Technology Conference*, pages 1087 –1091, 302007-oct.3 2007.

[43] Q. Zou, A. Tarighat, and A. Sayed. Joint compensation of IQ imbalance and phase noise in OFDM wireless systems. *IEEE Transactions on Communications*, 57(2):404 –414, 2009.

[44] J. Tubbax, B. Come, L. Van der Perre, S. Donnay, M. Engels, Hugo De Man, and M. Moonen. Compensation of IQ imbalance and phase noise in OFDM systems. *IEEE Transactions on Wireless Communications*, 4(3):872 – 877, May 2005.

[45] P. Rabiei, Won Namgoong, and N. Al-Dhahir. Reduced-Complexity Joint Baseband Compensation of Phase Noise and I/Q Imbalance for MIMO-OFDM Systems. *IEEE Transactions on Wireless Communications*, 9(11):3450 –3460, 2010.

[46] D. Hu, L. Yang, Y. Shi, and L. He. Optimal pilot sequence design for channel estimation in MIMO OFDM systems. *IEEE Communications Letters*, 10(1):1 – 3, January 2006.

[47] E.G. Larsson and J. Li. Preamble design for multiple-antenna OFDM-based WLANs with null subcarriers. *IEEE Signal Processing Letters*, 8(11):285 –288, November 2001.

[48] H. Minn and N. Al-Dhahir. Optimal training signals for MIMO OFDM channel estimation. *IEEE Transactions on Wireless Communications*, 5(5):1158 – 1168, May 2006.

[49] H. Minn, N. Al-Dhahir, and Yinghui Li. Optimal training signals for MIMO OFDM channel estimation in the presence of frequency offset and phase noise. *IEEE Transactions on Communications*, 54(10):1754 –1759, 2006.

[50] H. Minn and D. Munoz. Effect of I/Q Imbalance on Pilot Design for MIMO OFDM Channel Estimation. In *IEEE Global Telecommunications Conference*, pages 1 –5, 302009-dec.4 2009.

[51] H. Minn and D. Munoz. Pilot Designs for Channel Estimation of MIMO OFDM Systems with Frequency-Dependent I/Q Imbalances. *IEEE Transactions on Communications*, 58(8):2252 –2264, 2010.

[52] C. Oestges and B. Clerckx. *MIMO Wireless Communications: From Real-World Propagation to Space-Time Code Design*. Academic Press, Inc., Orlando, FL, USA, 2007.

[53] T. Rappaport. *Wireless Communications: Principles and Practice*. Prentice Hall PTR, Upper Saddle River, NJ, USA, 2nd edition, 2001.

[54] A. Goldsmith. *Wireless Communications*. Cambridge University Press, New York, NY, USA, 2005.

[55] J.P. Kermoal, L. Schumacher, K.I. Pedersen, P.E. Mogensen, and F. Frederiksen. A stochastic MIMO radio channel model with experimental validation. *IEEE Journal of Selected Topics in Signal Processing*, 20(6):1211 – 1226, August 2002.

[56] A. Van Zelst and J. S. Hammerschmidt. A single coefficient spatial correlation model for multiple-input multiple-output (mimo) radio channels. In *Proc. URSI XXVIIth General Assembly*, pages 1–4, 2002.

[57] I. Barhumi, G. Leus, and M. Moonen. Optimal training design for MIMO OFDM systems in mobile wireless channels. *IEEE Transactions on Signal Processing*, 51(6):1615 – 1624, june 2003.

[58] B. Driesen and TCW(Tim) Schenk. Backwards compatibility for MIMO systems based on IEEE 802.11a. In *Proc. 10th International OFDM - Workshop 2005, Hamburg, Germany,*, 2005.

[59] O. Edfors, M. Sandell, J.-J. van de Beek, S.K. Wilson, and P.O. Borjesson. OFDM channel estimation by singular value decomposition. *IEEE Transactions on Communications*, 46(7):931 –939, jul 1998.

[60] M. Belotserkovsky. An equalizer initialization algorithm for OFDM receivers. In *International Conference on Consumer Electronics*, pages 372 – 373, 2002.

[61] F. Marvasti, A. Amini, F. Haddadi, M. Soltanolkotabi, H. Khalaj, A. Aldroubi, S. Holm, S. Sanei, and J. A. Chambers. A Unified Approach to Sparse Signal Processing. *CoRR*, abs/0902.1853, 2009.

[62] M. Belotserkovsky. An equalizer initialization algorithm for IEEE802.11a and HIPERLAN/2 receivers. *IEEE Transactions on Consumer Electronics*, 48(4):1051 – 1055, nov 2002.

[63] Reuven Y. Rubinstein and Dirk P. Kroese. *Simulation and the Monte Carlo method (Wiley Series in Probability and Statistics)*. 2 edition.

[64] P.W. Wolniansky, G.J. Foschini, G.D. Golden, and R.A. Valenzuela. V-BLAST: an architecture for realizing very high data rates over the rich-scattering wireless channel. In *URSI International Symposium on Signals, Systems, and Electronics*, pages 295 –300, sep-2 oct 1998.

[65] R. Bohnke, D. Wubben, V. Kuhn, and K.-D. Kammeyer. Reduced complexity MMSE detection for BLAST architectures. In *IEEE Global Telecommunications Conference*, volume 4, pages 2258 – 2262 vol.4, dec. 2003.